ON SOME EXPERIMENTS WITH TIME DISCRETIZATIONS

O. Axelsson*)
CERN, Geneva, Switzerland

ABSTRACT

Different questions related to the numerical solution of parabolic equations have been studied[1]: i) the choice of the value θ in the θ-method, ii) the number of iterations in the solution of algebraic equations with matrix of the form $M + k(1-\theta)K$, M mass matrix, K stiffness matrix, both for linear and for non-linear problems.

1. MODEL PROBLEM

In order to investigate some numerical methods for the non-stationary electromagnetic field equation, we consider a model problem,

$$\frac{\partial u}{\partial t} = \frac{\partial}{\partial x_i}\left(a(|\nabla u|^2)\frac{\partial u}{\partial x_i}\right) + f(x,t,u) , \qquad x \in \Omega \subset R^n , \qquad (1.1)$$

where $a : R \to R$. For notational simplicity we assume that the boundary conditions are $u = 0$, $u \in \partial\Omega$. We assume a coercivity relation[2,3]

$$a(z) + \min\left\{0, 2\frac{\partial a}{\partial z}(z)z - \mu_1^{-1}\frac{\partial f}{\partial u}(u)\right\} \geq \delta > 0 , \qquad x \in \Omega , \quad (1.2)$$

where $z = |\nabla u|^2$ and where $\mu_1 = \mu_1(\Omega,-\Delta)$ is the smallest eigenvalue of the Laplacian operator $(-\Delta)$ on Ω or a positive lower bound thereof. We also assume that a and f are twice continuously differentiable with uniformly bounded derivatives.

This problem is discretized in space (R^2 or R^3) by some finite element approximation and in time by the simple θ-method,

$$u(t+k) - u(t) = k\frac{\partial}{\partial t}\left[(1-\theta)u(t+k)+\theta u(t)\right] , \qquad 0 \leq \theta \leq 1 .$$

The time-step k may be varied during the time-integration, and usually small steps are chosen during the transient phase.

2. ASYMPTOTIC ERROR ESTIMATES

Assume that the field equation (1.1) is approximated in space by some finite element method. This results in a system of ordinary differential equations on the variational form

$$(u_t,v) + (a(|\nabla u|^2)\nabla u,\nabla v) = (f(u),v) \qquad \forall\, v \in S_N , \qquad (2.1)$$

where S_N is a subspace of $\mathring{H}^1(\Omega) = \{u;\ \int_\Omega |\nabla u|^2\, dx < \infty,\ u = 0 \text{ on } \partial\Omega\}$. Here $(u,v) = \int_\Omega uv\, dx$.

*) On leave from Chalmers University of Technology, Göteborg, Sweden.

That (2.1) is equivalent to a system of N ordinary differential equations is made clear by letting $v = \phi_i$, $i = 1,2,\ldots,N$, the finite element basis functions, and $u(t,x) = \sum_{i=1}^{N} u_i(t)\phi_i(x)$, where $S_N = \text{SPAN}\{\phi_1,\phi_2,\ldots,\phi_N\}$. If we have chosen Lagrangian finite element functions, then $u_i(t)$ are the values of $u(t,x)$ at the nodal points.

In order to get a full discretization, we will use the so-called θ-method, where θ, $0 \leq \theta \leq 1$ is a parameter. There are two versions of this method (for linear problems, they are however equivalent).

$$\begin{aligned}&(U(t+k)-U(t),V) + k(1-\theta)(a(|\nabla U(t+k)|^2)\nabla U(t+k),\nabla V) + \\ &+ k\theta(a(|\nabla U(t)|^2)\nabla U(t),\nabla V) = \\ &= k((1-\theta)f(U(t+k))+\theta f(U(t)),V) \qquad \forall\, V \in S_N\end{aligned} \qquad (2.2)$$

and

$$\begin{aligned}&(U(t+k)-U(t),V) + k(a(|\nabla\bar{U}(t)|^2)\nabla\bar{U}(t),\nabla V) = \\ &= k(f(\bar{U}(t)),V) \qquad \forall\, V \in S_N\end{aligned} \qquad (2.3)$$

where

$$\bar{U}(t) = (1-\theta)U(t+k) + \theta U(t) .$$

For $\theta = \frac{1}{2}$, the first method is nothing but the trapezoidal (Crank-Nicolson) method and the second is the midpoint trapezoidal method[2]. We will derive an asymptotic error estimate of the second method. Since

$$(u(t+k)-u(t),v) = \int_t^{t+k} (u_t,v)\, dt = \int_t^{t+k} \left[(f(u),v) - (a(|\nabla u|^2)\nabla u,\nabla v)\right] dt$$

we get from (2.1)

$$\begin{aligned}&(u(t+k)-u(t),v) + k(a(|\nabla\bar{u}|^2)\nabla\bar{u},\nabla v) - k(f(\bar{u}),v) = \\ &= R_\theta(u,\nabla u;v,\nabla v) \qquad \forall\, v \in S_N ,\end{aligned} \qquad (2.4)$$

where

$$\begin{aligned}R_\theta(u,\nabla u;v,\nabla v) = k(a(|\nabla\bar{u}|^2)\nabla\bar{u},\nabla v) - \int_t^{t+k} (a(|\nabla u|^2)\nabla u,\nabla v)\, dt + \\ + k(f(\bar{u}),v) - \int_t^{t+k} (f(u),v)\, dt\end{aligned} \qquad (2.5)$$

Let $\Theta(t) = u(t) - U(t)$ be the time-discretization error. By subtracting (2.3) from (2.4) we get with $V = \bar{\Theta}(t)$,

$$(\Theta(t+k)-\Theta(t),\bar{\Theta}(t)) + k(a(|\nabla\bar{u}|^2)\nabla\bar{u}-a(|\nabla\bar{U}|^2)\nabla\bar{U},\nabla\bar{\Theta}) -$$

$$- k(f(\bar{u})-f(\bar{U}),\bar{\Theta}) = R_\theta(u,\nabla u;\bar{\Theta},\nabla\bar{\Theta}) \ .$$

However,

$$(a(|\nabla u|^2)\nabla\bar{u}-a(|\nabla\bar{U}|^2)\nabla\bar{U},\nabla\bar{\Theta}) - (f(\bar{u})-f(\bar{U}),\bar{\Theta}) =$$

$$= (a(|\nabla\bar{U}|^2)\nabla\bar{\Theta},\nabla\bar{\Theta}) + \left(\frac{\partial a}{\partial z}\,(|\nabla\bar{u}|^2-|\nabla\bar{U}|^2)\nabla\bar{u},\nabla\bar{\Theta}\right) - \left(\frac{\partial f}{\partial u}\,\bar{\Theta},\bar{\Theta}\right) \geq \delta|\nabla\bar{\Theta}|^2 > 0 \ ,$$

where we have used the assumption (1.2) and the fact that

$$\nabla v^T\nabla u\ \nabla u^T\nabla v = (\nabla v^T\nabla u)^2 \leq |\nabla u|^2\,|\nabla v|^2 \ .$$

We have also used

$$(\Theta,\Theta) \leq \mu_1^{-1}(-\Delta\Theta,\Theta) = \mu_1^{-1}(\nabla\Theta,\nabla\Theta) \ .$$

Hence

$$(\Theta(t+k)-\Theta(t),\bar{\Theta}) + k\delta\|\nabla\bar{\Theta}\|^2 \leq R_\theta(u,\nabla u;\bar{\Theta},\nabla\bar{\Theta}) \ . \qquad (2.6)$$

We have

$$\int_t^{t+k} g(v(s))\,ds - kg(\bar{v}(s)) = \int_t^{t+k} g(v(s))\,ds - kg(\tfrac{1}{2}[v(t+k)+v(t)]) +$$

$$+ k[g(\tfrac{1}{2}[v(t+k)+v(t)]) - g(\bar{v}(s))] = O(k^3)\,\frac{d^2}{dt^2}\,g(v(t)) - (\tfrac{1}{2}-\theta)k^2\frac{\partial g}{\partial v}\,\frac{dv}{dt} \ .$$

Hence, since a and t are twice continuously differentiable, by Cauchy-Schwarz inequality, we get from (2.5) and (2.6)

$$(\Theta(t+k)-\Theta(t),\bar{\Theta}) + k\delta\|\nabla\bar{\Theta}\|^2 \leq Ck^{-1}(O(k^3)+(\tfrac{1}{2}-\theta)O(k^2))^2 + \frac{k\delta}{2}\,\|\nabla\bar{\Theta}\|^2 \ ,$$

where C depends on δ and μ, but is independent of k. So

$$(\Theta(t+k)-\Theta(t),\bar{\Theta}) + \frac{k\delta}{2}\,\|\nabla\bar{\Theta}\|^2 \leq O(k^3)(O(k)+\tfrac{1}{2}-\theta)^2 \ .$$

An easy calculation shows that

$$(\Theta(t+k)-\Theta(t),\bar{\Theta}(t)) = \tfrac{1}{2}[\|\Theta(t+k)\|^2+(1-2\theta)\|\Theta(t+k)-\Theta(t)\|^2-\|\Theta(t)\|^2]$$

and

$$\|\bar{\Theta}(t)\|^2 = (1-\theta)\|\Theta(t+k)\|^2 - (1-\theta)\theta\|\Theta(t+k)-\Theta(t)\|^2 + \theta\|\Theta(t)\|^2 \ .$$

Hence

$$[1+k\delta'(1-\theta)]\|\Theta(t+k)\|^2 + \beta(\theta)\|\Theta(t+k)-\Theta(t)\|^2 \leq$$

$$\leq [1-k\delta'\theta]\|\Theta(t)\|^2 + O(k^3)(O(k)+\tfrac{1}{2}-\theta)^2 \ ,$$

where

$$\beta(\theta) = 1 - 2\theta - k\delta'(1-\theta)\theta \ , \qquad \delta' = \mu_1\delta \ .$$

We now choose θ such that

$$\beta(\theta) \geq 0 \ .$$

Hence $0 < \theta \leq \tfrac{1}{2} - |O(k)|$ and our final result is

$$\|\Theta(t+k)\|^2 \leq \alpha^{t/k+1}\,\|\Theta(0)\|^2 + \sum_{j=0}^{t/k} \alpha^{t/k-j}\,O(k^3)(\tfrac{1}{2}-\theta)^2 \ ,$$

where $\alpha = [1-k\delta'\theta]/[1+k\delta'(1-\theta)] < 1$. The initial error $\Theta(0) = 0$ if $U(0) = u(0)$. Hence, if $\theta = \tfrac{1}{2} - |O(k)|$ we have

$$\|u(t)-U(t)\| = O(k^2) \ , \qquad k \to 0 \ , \quad t > 0 \ .$$

This is the same asymptotic error estimate as for the Crank-Nicolson method, where $\theta = \tfrac{1}{2}$, but for the latter method the error estimate is not valid for all t, unless one imposes a restriction of k as a function of N. The above error estimate is however only an asymptotic error estimate valid as $k \to 0$ and assumes that there are no transients in the solution. It will follow that in the initial (transient) phase, one has to choose θ well below $\tfrac{1}{2}$, in order to be able to damp out these transients in the numerical solution.

3. CHOICE OF θ

In order to study the influence of θ on the actual error, we confine our study in this section to the simple linear problem

$$\frac{\partial u}{\partial t} = \frac{\partial^2 u}{\partial x^2} \ , \qquad x \in (0,1) \ ,$$

$$u(t,0) = u(t,1) = 0 \ , \quad t > 0 \ , \quad u(0,x) = u_0(x) \ .$$

By semi-discretization (in x) we get the system of ordinary differential equations

$$M\frac{du}{dt} + Ku = 0\ , \quad t > 0\ , \quad u(0) = u_0\ , \tag{3.1}$$

where $M = [(\phi_i,\phi_j)]$ is the mass matrix and $K = [(\phi_i',\phi_j')]$ is the stiffness matrix. In the numerical solution of (3.1) by the θ-method, we have

$$[M+k(1-\theta)K]\,U(t+k) = (M-k\theta K)\,U(t)\ , \qquad t = 0,k,2k,\ldots\ U(0) = U_0\ . \tag{3.2}$$

As is well known, the eigenvalues ρ of the matrix

$$[M+k(1-\theta)K]^{-1}\,(M-k\theta K)$$

which by similarity equals those of

$$[I+k(1-\theta)\tilde{K}]^{-1}\,(I-k\theta\tilde{K})\ , \qquad \tilde{K} = M^{-\frac{1}{2}}KM^{-\frac{1}{2}}\ ,$$

have to be ≤ 1, in order that the method is numerically stable. Let λ_q, $q = 1, 2, \ldots, N$, be the eigenvalues of $\tilde{K}$. Then

$$\rho_q = \rho(\theta,k\lambda_q) = (1-\theta k\lambda_q)/[1+(1-\theta)k\lambda_q]\ .$$

Since $|O(1)| \le \lambda_q \le O(N^2)$, we see that we have an unconditionally stable method (i.e. stable for all N), only if $\theta \ge \frac{1}{2}$. Let z_q be the orthonormal eigenvectors of $\tilde{K}$ and let

$$u_0 = U_0 = \sum c_q z_q\ , \quad \text{that is let } c_q = U_0^T z_q\ .$$

Then

$$u(t) = \sum_{q=1}^{N} c_q \exp(-\lambda_q t)\, z_q\ , \qquad U(t) = \sum_{q=1}^{N} c_q \rho_q^{t/k} z_q\ .$$

For the error

$$E(jk) = u(jk) - U(jk)\ ,$$

we get

$$E(jk) = \sum_{q=1}^{N} c_q \left[\exp(-k\lambda_q)-\rho_q\right] c_{qj}\, z_q\ , \tag{3.3}$$

$$c_{qj} = \sum_{\ell=0}^{j-1} \left[\exp(-\lambda_q k(j-1-\ell))\right] \rho_q^{\ell}\ .$$

Since $c_{qj} = O(1)$, $k \to 0$, and since $k\lambda_q > 0$, a simple strategy to get a small error component for all eigenvalues would be to choose θ such that

$$\min_{\theta} \max_{\lambda>0} \left|\exp(-\lambda)-\rho(\theta,\lambda)\right|\ .$$

is achieved. Then one gets $\theta = \theta_0 \approx 0.122$. However, this does not take the other factors into account, in particular the Fourier coefficients c_q, which in practical examples decrease with increasing λ_q. The rate of decrease of $|c_q|$ apparently depends on the smoothness of the initial function. For a function u_0 not satisfying the boundary conditions, we have an initial discontinuity, which leads to a slow decrease of c_q with q. Because of the exponential smoothing in u, the higher modes are damped out quickly however in the exact solution. To have them damped out quickly in the approximate solution U(t) we should choose θ close to 0. However, since the smaller modes have to be approximated reasonably well, which is done best with $\theta = \frac{1}{2}$, the optimal value of θ, making the total error as small as possible, lies in the open interval $(0,\frac{1}{2})$. We also realize that this value will be larger for a smoother function than for a less smooth function. This is confirmed by numerical tests[1]. The optimal value of θ varied between 0.13 - 0.40. However, the optimal value increases with j. This is so because for a fixed time t_0, the effective Fourier coefficients are [see (3.3)]

$$\tilde{c}_q = c_q \exp\left[-(1-\varepsilon)\lambda_q t_0\right]\ , \qquad 1 \le q \le q_0\ , \quad \varepsilon = \varepsilon(q_0)$$

corresponding to a problem with smoother initial function. The terms corresponding to the highest modes are small anyway if $\theta < \frac{1}{2}$, because

$$|\rho(\theta,\lambda)|^j \to \left|\left(\frac{\theta}{\theta-1}\right)^j\right| < 1\ , \qquad \lambda \to \infty\ .$$

From the discussion it follows that a good general strategy seems to be to choose $\theta \approx \frac{1}{3}$ for the first, say 5-10 integration steps. Then one lets $\theta = \frac{1}{2} - |O(k)|$ for the remaining steps, in order to get the asymptotic error $O(k^2)$.

4. SOLUTION OF LARGE SPARSE SYSTEMS OF EQUATIONS

At each step of the θ-method, we see from (3.2) that a generally large sparse system of algebraic equations, of the form

$$\tilde{M}\,U(t+k) = g(t)$$

where $\tilde{M} = M + k(1-\theta)K$, has to be solved. In order to preserve the sparseness, which is crucial in particular for three (space) dimensional problems, an iterative method, like the conjugate gradient method[4,5], can be applied. The rate of convergence of this method is determined by the smallest number ℓ, for which

$$2\,\frac{\sigma^{\ell}}{1+\sigma^{2\ell}} \le \varepsilon \ ,$$

where $\sigma = \left[1-\sqrt{\mu_1/\mu_0}\right]/\left[1+\sqrt{\mu_1/\mu_0}\right]$, μ_1 and μ_0 are the extreme eigenvalues of $\tilde{M}$, and ε is the relative accuracy demanded. An upper bound for ℓ is

$$\ell = \text{int}\left\{\frac{1}{2}\sqrt{\frac{\mu_0}{\mu_1}}\,\ln\frac{2}{\varepsilon}+1\right\} \ .$$

For not too large values of the condition number μ_0/μ_1, and $1/\varepsilon$, this estimate is too pessimistic and should be replaced by

$$\ell = \text{int}\left\{\ln\left(\frac{1}{\varepsilon}+\sqrt{\frac{1}{\varepsilon^2}-1}\right)\Big/\ln\frac{1}{\sigma}+1\right\} \ .$$

In particular, in the present context, the matrix $\tilde{N}$ has a fairly small condition number for all N, since M has a spectrum bounded by numbers independent of N and since the factor k makes the eigenvalues of the second term smaller. In particular, if $k = O(h^2)$, where h is the finite element average mesh size, then the condition number of $\tilde{M}$ is bounded by a number independent of N. Hence the conjugate gradient method makes the θ-method *effectively an explicit time-integration method*, in the respect that the number of operations per step is only O(N). This is discussed at some length in Ref. 1. In particular, one finds that in a model two-dimensional problem, the eigenvalues are clustered best for $k \approx \frac{1}{4}h^2$. The number of iterations was only two or three for a relative accuracy of $\varepsilon = 10^{-3}$, meaning a work of about 30 to 45 multiplications and additions per unknown.

Since in a time-dependent parabolic problem, we already have a good initial approximation at a new time-step, we do not need a particularly small relative accuracy.

In order to increase the rate of convergence further, which is of interest in the smooth region where k is usually O(h) [and hence[1,5] the number of iterations $O(h^{-\frac{1}{2}})$], we may use a preconditioned version of the method. Then one works with pseudoresiduals $\tilde{r}$, defined by

$$C\,\tilde{r} = r \ , \qquad r = \tilde{M}U(t+k) - g(t) \ .$$

The simplest choice of the preconditioning matrix C is the diagonal part of $\tilde{M}$, which helps to scale down the effect on the condition number of widely varying material coefficients. A more accurate preconditioning matrix results if we let C be an approximate factorization of M. Then C is chosen as the product of two triangular matrices, with as sparse, or almost as sparse, structure as the given matrix. Hence sparsity is still preserved and the number of operations per interative step in the conjugate gradient method is increased only slightly. Different choices of C are discussed in various papers[4,6].

Finally one observes that in a conjugate gradient method, the only use of the given matrix is as a factor in a matrix-vector multiplication. Hence it is enough to know the local small finite element matrices. By a proper choice of the mesh, most of these are equal, thereby implying a very small demand of storage.

Let us also mention that in the case of a periodic source function

$$f(x,t) = f_0(x)\,e^{i\omega t}$$

a linear problem

$$\frac{\partial u}{\partial t} = \frac{\partial}{\partial x_i}\left(a(x)\,\frac{\partial u}{\partial x_i}\right) + f$$

can be solved by a particular preconditioning technique, so that complex arithmetic is avoided, and sparsity is still preserved. The method is as follows: Since $u(x,t) = u_0(x)\,e^{i\omega t}$, we get

$$-\frac{\partial}{\partial x_i}\left(a(x)\,\frac{\partial u_0}{\partial x_i}\right) + i\omega u_0 = f_0$$

which after discretization has the form

$$(K+i\omega M)\,u_0 = f_0 \ .$$

Let $f_1 = \text{Re}\,(f_0)$, $f_2 = \text{Im}\,(f_0)$, $u_1 = \text{Re}\,(u_0)$. Then we have to solve

$$(K M^{-1} K + \omega^2 M)u_1 = K M^{-1} f_1 + \omega f_2$$

and this can be done iteratively by preconditioning by the matrix

$$C = (K+\omega M)\,M^{-1}\,(K+\omega M) \ .$$

One can easily show[5], that the resulting condition number of the iteration matrix

$$C^{-1}\,(K M^{-1} K+\omega^2 M)$$

is < 2, for all positive semi-definite matrices K. The linear systems with matrix $K + \omega M$ may be solved by a preconditioned conjugate gradient method as has already been described.

5. NUMBER OF ITERATIONS FOR THE NON-LINEAR PROBLEM

Let us now consider the non-linear problem (1.1). We shall study the number of iterations needed at each time-step. Hence it suffices to consider just one time-step $0 \to k$. The variational formulation of (1.1) using the θ-method (2.3) is then

$$(U(k)-U(0),V) + k(a(|\nabla\bar{U}(k)|^2)\nabla\bar{U},\nabla V) = k(f(\bar{U}),V) \qquad \forall V \in S_N \,. \tag{5.1}$$

It is easily seen that this expression is the gradient of the functional

$$F(U(k)) = \frac{1}{2}\|U(k)-U(0)\|^2 + \frac{k}{1-\theta}\int_\Omega \left[\frac{1}{2}\int_0^{|\nabla\bar{U}(k)|^2} a(\zeta)d\zeta - \int_0^{\bar{U}} f(\xi)d\xi\right]$$

and the solution U(k) will be the (unique) minimizer of this functional. Hence[7] we may again apply a conjugate gradient iterative method to minimize F. We may also use a Newton method to solve (5.1). It is however easily realized[7] that this latter method is equivalent to successively approximate the functional $F(U(k))$ by a quadratic functional based on the Hessian matrix $F'' = H(|\nabla\bar{U}|^2)$ of F, evaluated at $\nabla\bar{U}^{(\ell)}$, $\ell = 0, 1, \ldots$, the approximation found at the previous iteration. To solve for the minimizer of the quadratic functional, we may apply a (preconditioned) conjugate gradient method. If we use a preconditioning of the conjugate gradient method, the preconditioning matrix is usually also based on the Hessian. Thus we see that there is a close relationship between the Newton method and the preconditioned conjugate gradient method.

However, since it is costly to re-evaluate the Hessian (second derivative) matrix, one may instead use an approximation of it, derived from having approximated a and f as locally constant over each local finite element. Then one does not have to repeat the numerical integrations. One may also divide the given region into subregions and neglect updating of the local finite element matrices in calm zones[7], where only a minor change in the gradients and the solution has occurred from previous iterative steps. Similarly, one can use a modified Newton method, where the Hessian is only partly updated.

One finds[1] in the present context that even in a problem with a high degree of non-linearity, the number of conjugate gradient steps is not more than 3 or 4 times that in the corresponding linear problem. At each conjugate gradient step, it was found that the additional cost of making line searches, did not pay off. The number of Newton steps was smaller, but since the cost of each Newton step is equivalent to the number of conjugate gradient steps for a linear problem, in general the Newton method does not lead to a smaller total computational cost. Only where the initial approximation is so accurate, that the Newton method only needs two or three steps for convergence, will this method be more advantageous.

One interesting result[1] was that in some cases, notably when θ was close to $\frac{1}{2}$, the actual error in the numerical solution (which consists of a discretization and an iteration error), when making only one Newton iteration, was smaller than the error after making full iteration (when the iteration error is negligible).

REFERENCES

1. Axelsson, O and Steihaug, T, Some computational aspects in the numerical solution of parabolic equations, J. Comput. Appl. Math. 4, 129-142, 1978.

2. Axelsson, O, Error estimates for Galerkin methods for quasi-linear parabolic and elliptic differential equations in divergence form, Numer. Math. 28, 1-14, 1977.

3. Axelsson, O, On the numerical solution of non-linear partial differential equations on divergence form, Equadiff 4, Prague, August 1977.

4. Axelsson, O, A class of iterative methods for finite element equations, Comput. Methods Appl. Mech. Engrg. 9, 123-137, 1976.

5. Axelsson, O, On preconditioned conjugate gradient methods, Technical report, Center for Numerical Analysis, The University of Texas at Austin, 1978.

6. Gustafsson, I, A class of first order factorization methods, BIT 18, 142-156, 1978.

7. Axelsson, O and Nävert, U, On a graphical package for non-linear partial differential equation problems, Proc. IFIP Congress 77 (Ed. B. Gilchrist), IFIP, North-Holland, 1977.

CALCUL TRIDIMENSIONNEL DES COURANTS DE FOUCAULT DANS UN SOLIDE NON FERROMAGNETIQUE

J. C. VERITE
E.D.F. Etudes et Recherches 1 av. du Général De Gaulle
92141 CLAMART

RESUME

Un solide parallélépipédique est soumis à un potentiel-vecteur inducteur dû à un circuit électrique extérieur. Le solide est décomposé en cubes élémentaires, tous de mêmes dimensions, sur les faces desquels la densité de courant est supposée constante. La discrétisation des équations de Maxwell résolues par rapport à la densité de courant fournit alors un système linéaire dont les inconnues sont pour chaque face la densité de courant et pour chaque cube le potentiel scalaire en son centre. Les problèmes d'encombrement et de temps de résolution du système sont mis en évidence ainsi que les limites d'une approche directe et globale d'un problème tridimensionnel.

1. INTRODUCTION

La géométrie (fig.1) est constituée d'un solide conducteur parallélépipédique Ω. Il est non ferromagnétique. Il est seul dans l'espace avec un circuit électrique quelconque situé à son voisinage et dont le seul rôle est de créer un potentiel-vecteur inducteur sinusoïdal au sein de Ω. On se propose de trouver la répartition de courant induit dans Ω.

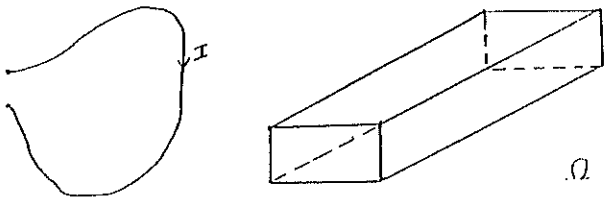

Fig. 1

2. MISE EN EQUATIONS

Soit a_o le potentiel-vecteur inducteur, a le potentiel-vecteur global, j la densité de courant dans Ω, φ le potentiel scalaire et σ la conductivité de Ω. e, b et h sont respectivement le champ électrique, l'induction magnétique et le champ magnétique. Toutes les grandeurs électriques sont sinusoïdales de pulsation ω.

Dans Ω nous avons les équations suivantes :

$$\text{rot } e + \frac{\delta b}{\delta t} = 0 \qquad \text{(Maxwell)} \tag{1}$$

$$\text{roth} = j \qquad \text{(Maxwell)} \tag{2}$$

$$j = \sigma e \qquad \text{(Ohm)} \tag{3}$$

$$b = \text{rot } a \text{ avec div } a = 0 \text{ (Définition du potentiel-vecteur)} \tag{4}$$

$$\text{div} j = 0 \text{ (conservation de la charge électrique)} \tag{5}$$

$$b = \mu h \tag{6}$$

Les équations (1) et (4) donnent : $\text{rot}\left(e + \frac{\delta a}{\delta t}\right) = 0$

soit $e + \frac{\delta a}{\delta t} = \text{grad } \varphi$

soit en régime harmonique dans Ω :

$$i\omega a + \sigma^{-1} j = \text{grad } \varphi \tag{7}$$

D'autre part, (2) et (6) donnent : rot rot a = μj

Soit puisque div a = 0 :

$$\Delta a = -\mu j \text{ dans } \Omega \tag{8}$$

dont la solution formelle est bien connue :

$$a(x) = \frac{\mu}{4\pi} \int_{\Omega} \frac{j(y)}{|x-y|} d\Omega y + a_o(x) \tag{9}$$

Pour calculer j dans Ω, il nous faut résoudre le système constitué des équations (5), (7) et (9).

3. DISCRETISATION DES EQUATIONS

Le solide est décomposé en cubes élémentaires $d\omega_i$ sur les faces f_{ij} desquels la densité de courant J_{ij} sera supposée constante. On cherchera alors à calculer la composante normale $J_{nij} = j_{ij}$ de cette densité de courant sur chaque face (fig. 2).

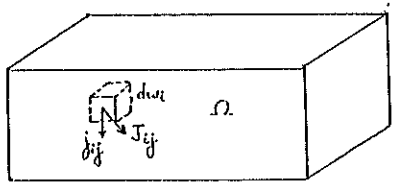

Fig. 2

Soit nc le nombre de cubes et nf le nombre de faces actives, c'est-à-dire n'appartenant pas à la frontière de Ω sur laquelle J. n = 0. L'indice i se rapportant aux cubes et l'indice k aux faces, exprimons a_n = a.n et j = J. n au centre des faces et φ au centre des cubes.

L'équation (5) devient, pour i variant de 1 à nc :

$$\sum_k j_{ik}.S = 0 \quad S \text{ étant la surface de chaque face.}$$

Cette équation exprime que le flux total de densité de courant sortant de chaque cube élémentaire est nul.

Soit D étant une matrice ncxnf :

$$Dj = 0 \qquad (10)$$

Pour discrétiser l'équation (9), il faut considérer que le support de la densité de courant j_k de la face k est un cube c_k décalé par rapport au maillage, centré sur la face k (fig. 3)

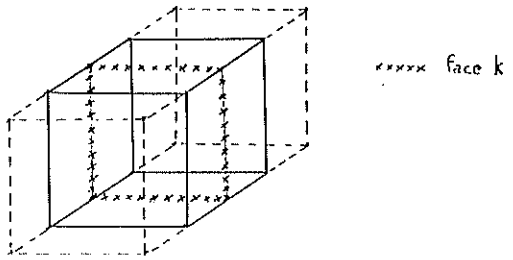

Fig. 3

(9) s'écrit :

$$a_n(x_i) = \frac{\mu}{4\pi} \sum_{j=1}^{nf} \int_{c_j} \frac{j(y_j).n_i}{|x_i - y_j|}\, dC_j + a_{on}(x_i)$$

Pour i ≠ j, Mi et Mj étant les centres des cubes décalés Ci et Cj, on prend :

$$\int_{c_j} \frac{j(y_j).n_i}{|x_i - y_j|}\, dC_j = \frac{j_j(Mj).n_i.V}{|Mi\ Mj|}$$

.V étant le volume d'un cube élémentaire.

Pour i = j, l'intégrale est singulière. On calcule une valeur moyenne prise sur le cube :

$$\frac{1}{v} \int_{C_i} \int_{C_i} \frac{j(y_i)}{|x_i - y_i|}\, dC_i\, dC_i$$

L'intégrale intérieure est calculée numériquement par une formule à 6 points et l'intégrale extérieure par une formule à 9 points (cf. [2])

(9) devient alors, a, a_o et j étant des composantes normales pour simplifier l'exposé :

$$a = Gj + a_o \qquad (11)$$

où G est une matrice carrée nf x nf

Enfin dans l'équation (7), il reste à discrétiser grad φ dont les valeurs doivent être prises au centre des faces. On fait grad φ.n = $\varphi_i - \varphi_j$, φ_i et φ_j étant les valeurs de φ au centre des cubes adjacents à la face considérée.

$$\text{Soit } i\omega a + \sigma^{-1} j = S\varphi \quad S \text{ matrice nf x nc} \qquad (12)$$

(11) et (12) donnent : $i\omega (Gj + a_o) + \sigma^{-1} j = S\varphi$

$$\text{Soit } (i\omega G + \sigma^{-1} I)j - S\varphi = - i\omega a_o \qquad (13)$$

Remarque :

$$\int_\Omega j.\ \mathrm{grad}\varphi\, d\Omega + \int_\Omega \mathrm{div} j.\varphi\, d\Omega = \int_{\partial\Omega} \varphi.j.n.d\partial\Omega$$

∂Ω étant la frontière deΩ

Soit, puisque j.n = 0 sur ∂Ω : $j^t S\varphi + \varphi^t Dj = 0$

donc $S = - D^t$, transposée de − D

Le système d'équations discrétisées à résoudre est donc le suivant :

$$\begin{cases} (i\omega G + \sigma^{-1} I)\ j + D^t\varphi = - i\omega a_o \\ Dj = 0 \end{cases}$$

Il s'agit d'un système linéaire complexe symétrique de dimension nf + nc = n à nf inconnues j et nc inconnues φ :

$$\begin{pmatrix} H & D^t \\ D & 0 \end{pmatrix} \begin{pmatrix} j \\ \varphi \end{pmatrix} = \begin{matrix} f \\ 0 \end{matrix}$$

4. RESOLUTION DU SYSTEME

4.1. Difficultés dues au caractère tridimensionnel du problème

Pour simplifier l'exposé, supposons que le parallélépipède soit un cube. Soit N le nombre d'intervalles de discrétisation suivant

chacune des arêtes du cube. Le tableau suivant donne, en fonction de N, la taille n du système à résoudre.

N	nombre de faces nf	nombre de cubes nc	n
2	12	8	20
4	144	64	208
10	2700	1000	3700

nf représente la taille de la sous-matrice H du système à résoudre, H étant complexe et ayant la structure suivante :

$$H = \begin{pmatrix} Hx & 0 & 0 \\ 0 & Hy & 0 \\ 0 & 0 & Hz \end{pmatrix}$$

où Hx représente les faces perpendiculaires à l'axe des x. Hx, Hy, et Hz sont symétriques, mais sont pleines et complexes. Dans le cas N = 10 chacune d'elles est de dimension 900. La sous-matrice D est très creuse et pose moins de problèmes. Néanmoins, on voit que pour ce cas on a déjà très largement dépassé les capacités de la mémoire centrale (1000 K pour l'IBM 370-168 sur laquelle cette étude a été effectuée).

D'autre part, même en employant une méthode itérative pour la résolution du système, pour laquelle on peut sans difficulté appeler la matrice en mémoire centrale ligne par ligne ou groupe de lignes par groupe de lignes, des temps de convergence non prohibitifs vont nous limiter à N inférieur à 10 comme nous allons le voir.

4.2 Description de la méthode itérative utilisée

La structure de la matrice fait apparaître un certain nombre de termes diagonaux nuls. Ceci interdit l'emploi pour la matrice globale des méthodes habituelles de Gauss-Seidel, Jacobi ou de relaxation.

La méthode du gradient conjugué, qui donne la solution exacte en N itérations pour un système de dimension N, converge trop lentement au cours des premières itérations.

En fait, les inconnues φ sont des multiplicateurs de Lagrange et nous avons adopté un processus itératif différent pour les j et pour les φ, tenant compte de leur dissymétrie dans le système.

Le système peut s'écrire : $\begin{cases} Hj + D^t\varphi = f \\ Dj = 0 \end{cases}$

Soit $j = H^{-1}f - H^{-1}D^t\varphi$ ou $Dj = DH^{-1}f - DH^{-1}D^t\varphi$, qui est le gradient de $\langle H^{-1}f, D^t\varphi \rangle - \frac{1}{2} ||DH^{-1}D^t\varphi||^2$, expression analogue à une énergie.

Dans ces conditions, nous allons utiliser une méthode de relaxation ponctuelle pour j et une méthode du gradient pour φ.

L'algorithme est le suivant, où n est le numéro de l'itération en cours, ℓ l'indice de ligne et k l'indice de colonne. $h_{\ell k}$ et $d_{\ell k}$ sont les termes de H et D, leurs indices étant rapportés à leur position dans la matrice globale.

Pour $1 \leq \ell \leq nf$:

$$h_{\ell\ell} \hat{j}_\ell^{n+1} = f - \sum_{k=1}^{\ell-1} h_{\ell k} j_k^{n+1} - \sum_{k=\ell+1}^{nf} h_{\ell k} j_k^{n} - \sum_{k=nf+1}^{nf+nc} d_{k\ell} \varphi_k^{n}$$

$$\text{et } j_\ell^{n+1} = j_\ell^{n} + \omega(\hat{j}_\ell^{n+1} - j_\ell^{n})$$

Pour $nf < \ell \leq nf + nc$:

$$\varphi_\ell^{n+1} = \varphi_\ell^{n} - \rho d_{\ell k} j_k^{n+1}$$

5. RESULTATS

Pour tous les résultats que nous allons donner, Ω est un cube de côté L = 2,4 cm et le support du courant appliqué I est un anneau C de rayon 2L centré au centre du cube. Les constantes électriques de Ω sont celles de l'aluminium. Dans ce qui suit les arêtes de Ω sont dirigées suivant les axes Ox, Oy, Oz.

Le tableau suivant indique pour chaque cas étudié la fréquence du phénomène, le nombre N de cubes élémentaires suivant une arête de Ω, le plan de C, les valeurs de ω et ρ, le nombre d'itérations NI, la valeur

$$\varepsilon = \frac{\max_i |\alpha_i^{n+1} - \alpha_i^{n}|}{\max_j |\alpha_j^{1} - \alpha_j^{0}|} \quad \text{pour } n = NI \text{ (test de convergence)}$$

et enfin le temps CPU

N° essai	N	fH_z	plan de C	ω	ρ	ε	NI	Tcpu
1	4	50	z = D/2	1.	.07	.25E-04	88	32s
2	6	50	z = D/2	.4	.03	.85E-04	88	4mn14s
3	6	250	z = D/2	.4	.03	.13E-03	88	4mn 9s
4	6	50	y = z	1.	.06	.27E-02	88	4mn12s
5	8	50	y = D/2	.4	.03	.74E-03	88	23mn8s

Les diagrammes suivants montrent les résultats obtenus en prenant au centre de chaque cube élémentaire la moyenne des courants normaux au centre de chacune de ses faces.

Le plan de figure est le plan x0y. L'axe des z est en perspective suivant x = y et son échelle est dilatée pour qu'il y ait le moins de chevauchement possible. Les parties restant malgré tout cachées sont supprimées.

Pour chaque essai, φ étant le déphasage par rapport à l'origine de phase du courant inducteur I, on donne les résultats pour $\varphi = 0$ et $\varphi = \pi/2$. Dans chaque cas on donne deux diagrammes : l'un représente la projection du courant sur le plan x0y de figure et l'autre la projection suivant l'axe des z. Les échelles ne sont pas les mêmes dans les deux cas. m est le rapport entre l'échelle suivant 0z et l'échelle suivant x0y.

Il y a donc 4 vues pour chaque cas. Pour des raisons de place nous ne donnons ici que les diagrammes des essais 2, 3 et 4. La partie supérieure de chaque diagramme représente les courants suivant x0y et la partie inférieure ceux suivant 0z.

Figure 4 : Essai 2 $\varphi = 0$ m = 131

Figure 5 : Essai 2 $\varphi = \pi/2$ m = 131

Figure 6 : Essai 3 $\varphi = 0$ m = 98,6

Figure 7 : Essai 3 $\varphi = \pi/2$ m = 98,6

Figure 8 : Essai 4 $\varphi = 0$ m = 1,33

Figure 9 : Essai 4 $\varphi = \pi/2$ m = 1,33

6. CONCLUSIONS

Nous avons arbitrairement arrêté l'algorithme à 88 itérations. Pour N = 4 (essai n° 1) la convergence est très bonne. Pour N = 6 et f = 50 Hz (essai n° 2) elle est encore très convenable. Notons qu'en augmentant la fréquence (essai n° 3) elle est un peu moins bonne. Ceci est sans doute dû au fait que le courant se concentrant à la frontière de Ω, la solution est plus irrégulière. Pour les essais 4 et 5 la convergence est nettement moins bonne. Pour l'essai 5 en particulier, pour lequel les courants suivant l'axe des z sont beaucoup plus faibles que ceux du plan x0y, ces courants faibles sont entâchés d'assez grosses erreurs relatives. De plus les 88 itérations ayant dans ce dernier cas pris 25 mn de temps CPU sur IBM 370-168, on voit que cette approche globale des problèmes tridimensionnels se heurte à de grosses difficultés.

BIBLIOGRAPHIE

[1] R.L. STOLL - The analysis of eddy currents. Clarendon-Press - Oxford 1974.

[2] A.H. STROUD - Approximate calculation of multiple integrals. Prentice-Hall - 1971.

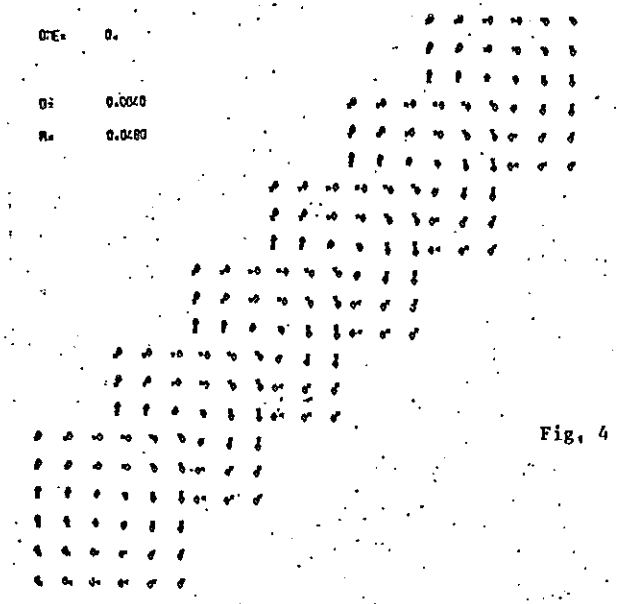
DIE= 0.
D= 0.0000
R= 0.0480

Fig. 4

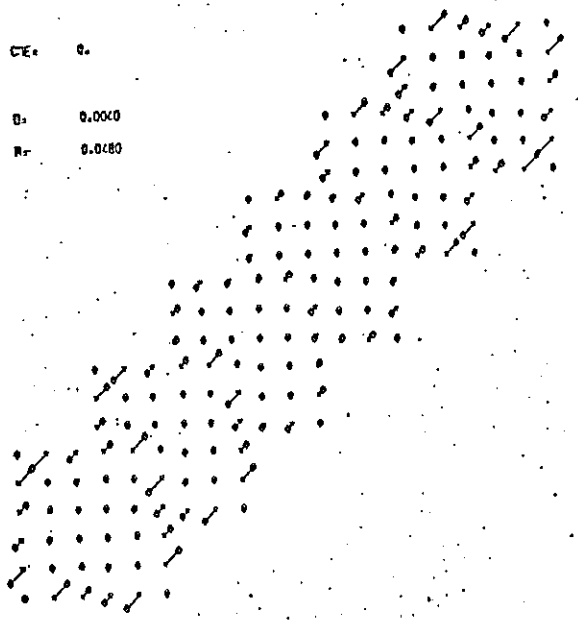
DIE= 0.
D= 0.0000
R= 0.0480

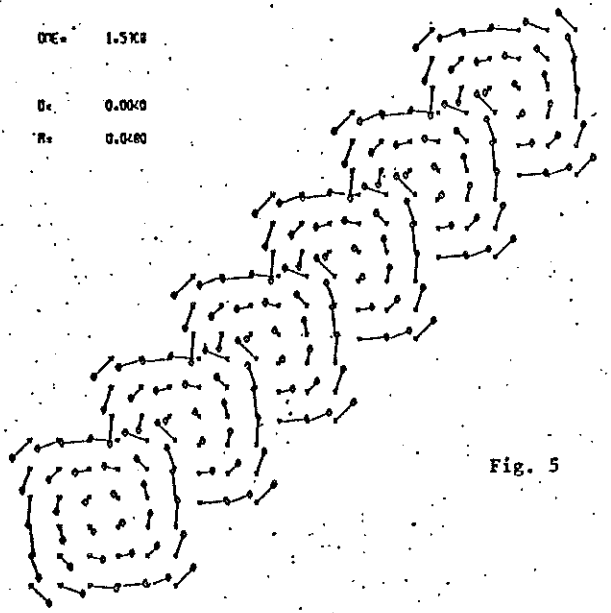
DIE= 1.5708
D= 0.0000
R= 0.0480

Fig. 5

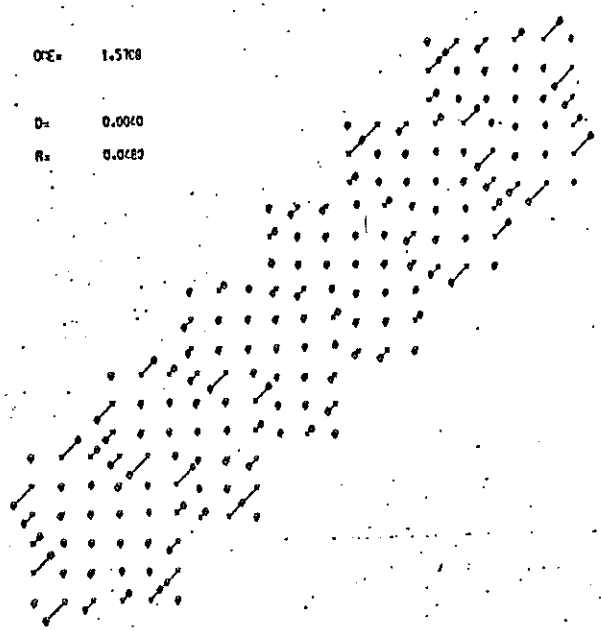
DIE= 1.5708
D= 0.0000
R= 0.0480

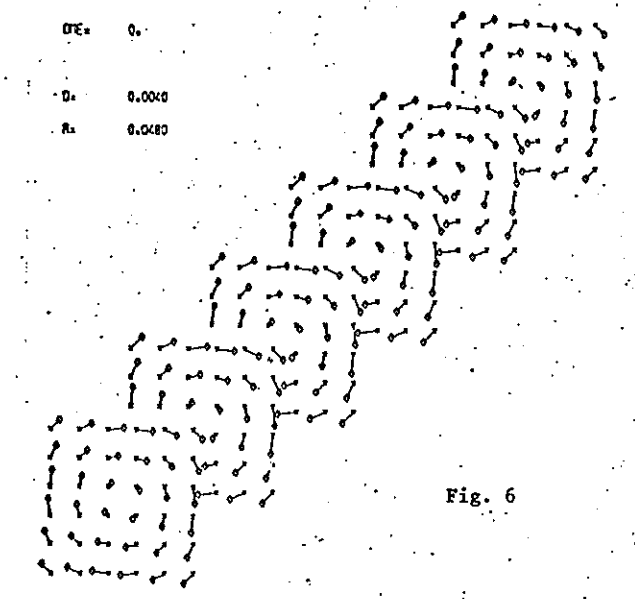
0.
0.0000
0.0480

Fig. 6

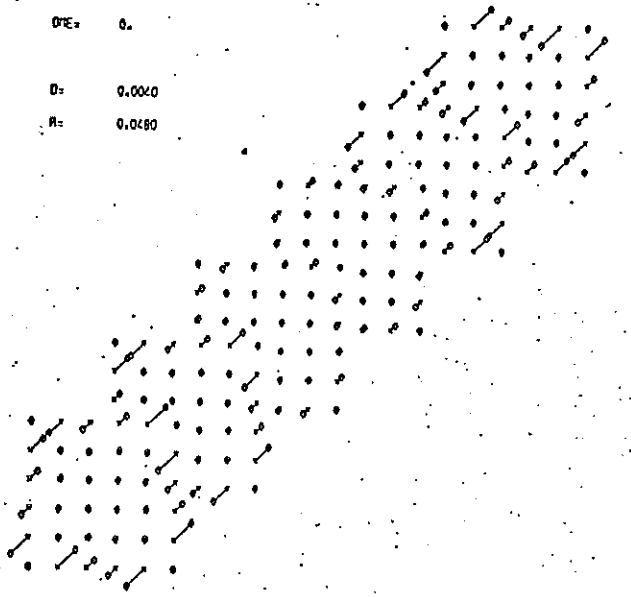
0.
0.0000
0.0480

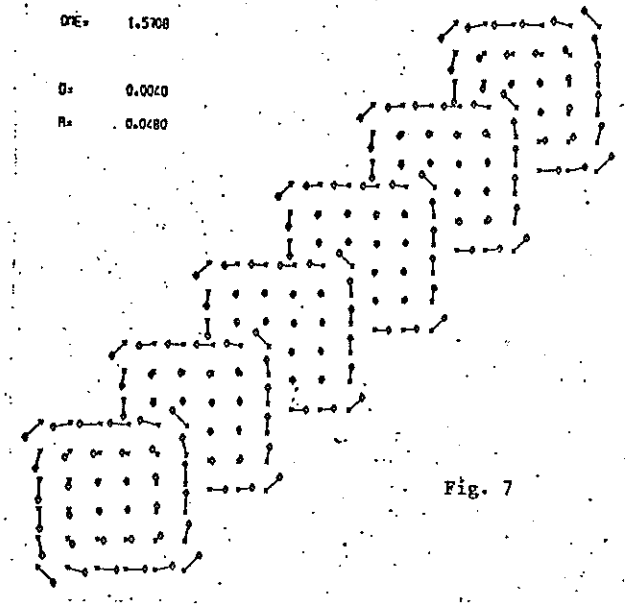
1.5708
0.0000
0.0480

Fig. 7

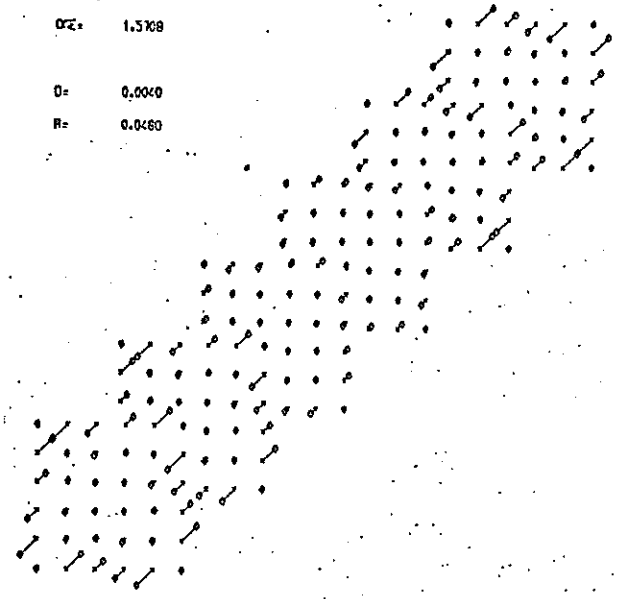
1.5708
0.0000
0.0480

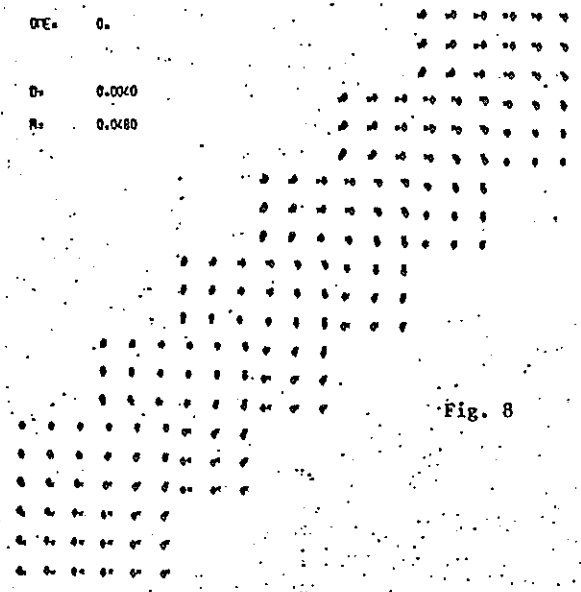
0.
0.0000
0.0480

Fig. 8

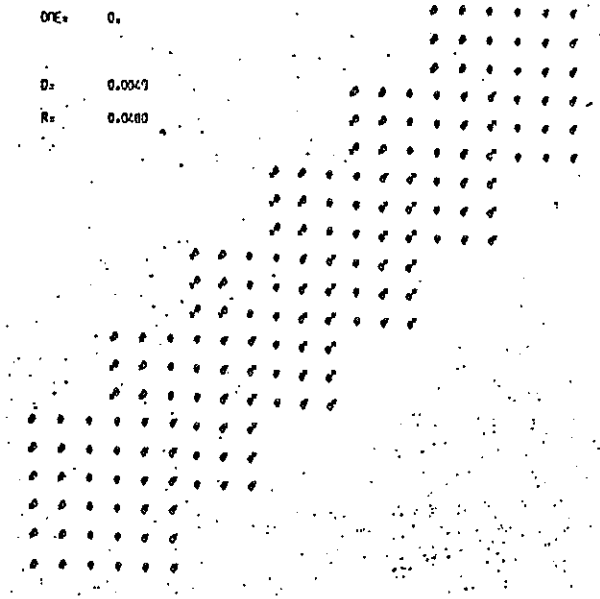
0.
0.0000
0.0480

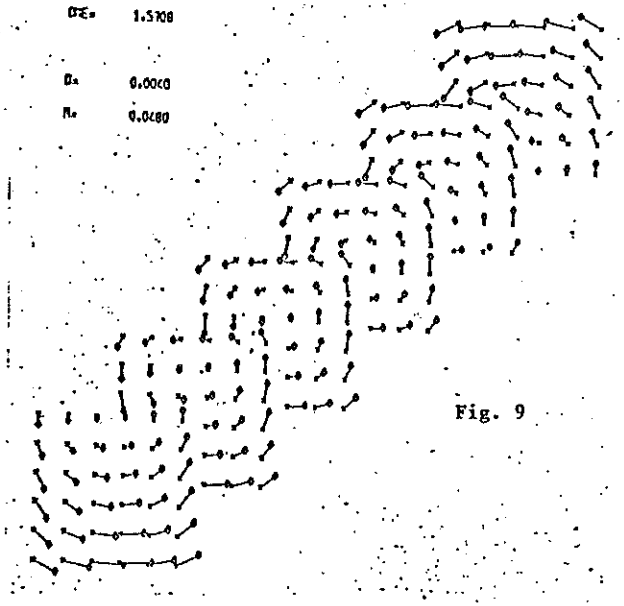
1.5708
0.0000
0.0480

Fig. 9

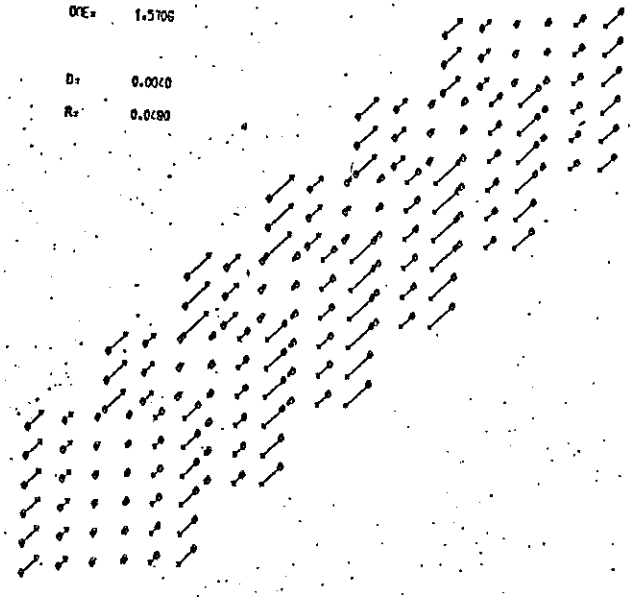
1.5708
0.0000
0.0480

FINITE-ELEMENT SOLUTION OF 3-DIMENSIONAL EDDY CURRENT PROBLEMS IN ELECTRICAL MACHINES

T.W. Preston and A.B.J. Reece
Stafford Laboratory, G.E.C. Power Engineering Ltd.,
Lichfield Road, Stafford, ST17 4LN.

ABSTRACT

The development of large machines has high-lighted a number of eddy current problems where a full 3-dimensional treatment is required.

This paper describes a finite-element method applicable to full 3-dimensional eddy current problems, although only planar flow of induced currents in a 3-dimensional geometry is considered in detail. The work is based on the T (electric vector potential) - Ω (magnetic scalar potential) method, and, to obtain confidence in the approach, comparison is made on a problem for which an analytic solution is possible. The effect of discretisation, and the importance of boundary specification at interfaces are illustrated.

1. INTRODUCTION

Many electromagnetic problems in electrical machines can be tackled effectively by making 2-dimensional approximations to the real 3-dimensional situation. However, because of higher specific ratings and more onerous operating conditions, there are an increasing number of cases where solution of 3-dimensional eddy current problems is essential. Examples arise in negative-sequence heating of turbine-generator rotors, and in the starting of solid salient-pole machines with bolted-on pole-heads.

This work started by consideration of methods which might be applicable to the solution of 3-dimensional problems, and particular attention was given to the use of the magnetic vector potential. It was found that this approach raised considerable difficulties in the treatment of interface conditions between conducting and non-conducting members: also, all three components of vector potential had to be derived throughout the problem, together with a scalar potential in the conducting medium, thus increasing the cost of computation. After investigating a current density formulation, which proved to be inadequate for the problems of interest, it was decided to develop the T (electric vector potential) - Ω (magnetic scalar potential) method: this has the attraction that T has only to be calculated in conducting regions. For the general case of three current components, two components of T are sufficient, and for current flow in planes, only one component of T is needed. The T - Ω method has been described by Carpenter in Refs. 1 and 2, and a variation by Wolff is introduced in Ref. 3.

This paper describes the development of a "one-T" - Ω approach in 3-dimensional space, and compares results for a simplified case with those obtained analytically. The finite-element solution method is used, but since its application to T - Ω problems is new, insight into the effect of different treatments of interfacial conditions, etc., was obtained by assuming analytic variations in two directions, with variations occurring in the direction of the single T-vector treated numerically.

Finally, the practical problem of calculating the current flow in and around the junction between wedges of a turbine-generator rotor is considered. Extension of the equations for a "two-T" - Ω approach is described.

2. FORMULATION OF T - Ω EQUATIONS

The T - Ω approach divides the problem into two parts, viz.: (a) determination of the magnetic scalar potential (Ω), which defines the magnetic field distribution (with some modification by T in conducting regions), and (b) determination of the electric vector potential (T), which describes the current flow patterns in the conductor region. The electric vector potential can be regarded as a generalised variation of the H formulation, in that it has the same "curl" relationship, but not necessarily the same divergence:

i.e. $\text{Curl } H = J$ ..... (1)

and $\text{Curl } T = J$ ..... (2)

Since $\text{div } \mu H = 0$ ..... (3)

H can be re-defined in terms of T and Ω as:

$$H = T - \text{grad } \Omega \qquad \ldots\ldots (4)$$

which, if operated on by the "curl", satisfies Eqns. (1) and (2).

The magnetic scalar potential equation is obtained from Eqns. (3) and (4), and can be expressed as:

$$\mu \left\{ \frac{\partial^2 \Omega}{\partial x^2} + \frac{\partial^2 \Omega}{\partial y^2} + \frac{\partial^2 \Omega}{\partial z^2} \right\} = \mu \text{ div } T \qquad \ldots\ldots (5)$$

(The permeability terms need to be retained to allow for materials of different permeability in the numerical formulation.)

The equation for the electric vector potential (T) is given by Maxwell's equation:

$$\text{Curl } E = -\frac{\partial B}{\partial t} \qquad \ldots\ldots (6)$$

and $\text{Curl } T = J$ ..... (7)

The resulting expression is:

$$\nabla \times (\rho \nabla \times T) = -\frac{\partial B}{\partial t} \qquad \ldots\ldots (8)$$

In the early stages of the work only one component of T, (T_x), is assumed, which corresponds to planar flow of current: it is also

assumed that all materials have constant permeability and resistivity. Thus, for sinusoidal time variations in both potentials, Eqns. (5) and (8) reduce to:

$$\mu \left\{ \frac{\partial^2 \Omega}{\partial x^2} + \frac{\partial^2 \Omega}{\partial y^2} + \frac{\partial^2 \Omega}{\partial z^2} \right\} = \mu \frac{\partial T}{\partial x} \qquad \ldots\ldots\ (9)$$

and

$$\rho \left\{ \frac{\partial^2 T}{\partial y^2} + \frac{\partial^2 T}{\partial z^2} \right\} = j\,\omega\,\mu \left\{ T - \frac{\partial \Omega}{\partial x} \right\} \qquad \ldots\ldots\ (10)$$

where the x-direction is normal to the conducting surface.

Since T is a current-describing function, i.e. a function from which J can be derived by differentiating in accordance with Eqn. (2), T is either zero or a constant in non-conducting regions. Thus Eqn. (10) is only evaluated in conducting regions, whereas Eqn. (9) is evaluated throughout.

Numerical solution of the above equations is necessary for the complicated boundary shapes which arise in electrical machines. Since our experience with 2-dimensional problems has shown the finite-element method to be well-suited to economic solution for awkward geometries, it has been adopted for the solution of Eqns. (9) and (10).

In the absence of any published work on finite-element solution of 3-dimensional eddy current problems, a cautious approach was adopted. This involved the finite-element solution of Eqns. (9) and (10), assuming the variation in the y- and z-directions to be sinusoidal and co-sinusoidal respectively. Thus the numerical solution is in one dimension only (the x-direction), and, as shown in the following section, the effect of interface conditions and discretisation can be examined in detail at modest computational cost.

3. ANALYTIC AND NUMERIC FORMULATION OF THE SINGLE T - Ω SOLUTION

3.1 General

To dispel any doubts about the variational formulation, and to clarify the effects of interface relationships and discretisation, it is essential to test the validity of the approach on a problem for which an analytic solution is possible. A test problem was set up (Fig. 1), which simulated a simple stator and rotor assembly. The following assumptions have been made so that an analytic solution can be obtained:-

(i) The stator core is infinitely permeable.

(ii) The rotor material is assumed to have constant permeability.

(iii) The sinusoidally varying stator currents set up a magnetic scalar potential on the stator surface having a sinusoidal variation in the y-direction and a co-sinusoidal variation in the z-direction.

(iv) The electric vector potential distribution in the rotor is similarly distributed.

Boundary conditions are indicated in Fig. 1.

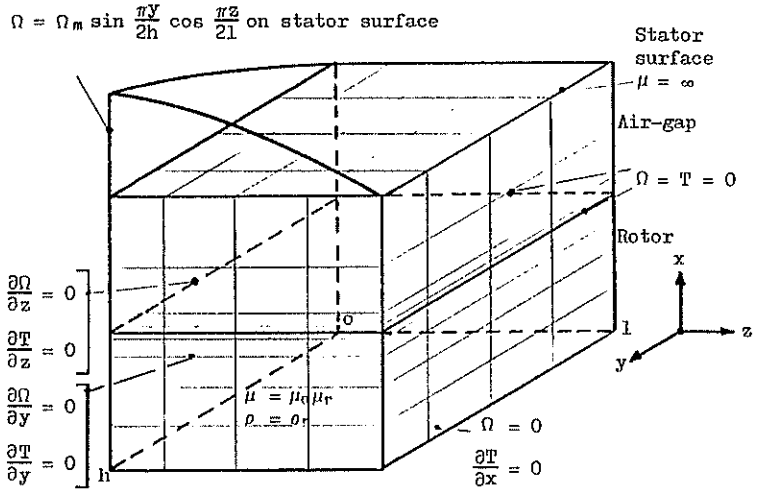

Fig. 1: Simplified stator and rotor assembly

3.2 Analytic Solution

When all the assumptions are considered, the problem reduces to Fig. 2:

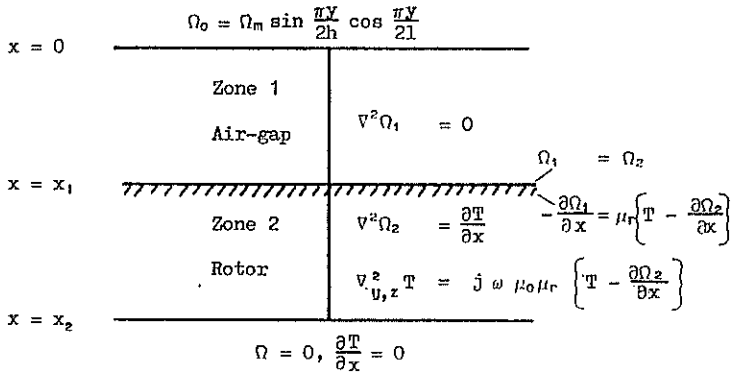

Fig. 2: Mathematical model of Fig. 1

∴ Let $\Omega_0 = \Omega \sin \frac{\pi y}{2h} \cos \frac{\pi z}{2l}$ ..... (11)

and $T_0 = T \sin \frac{\pi y}{2h} \cos \frac{\pi z}{2l}$ ..... (12)

which, when substituted into Eqns. (9) and (10), give:

In Zone 1: $\frac{\partial^2 \Omega_1}{\partial x^2} - K \Omega_1 = 0$ ..... (13)

where $K = \frac{\pi^2}{4l^2 h^2} (h^2 + l^2)$

$$T = 0 \qquad \ldots\ldots (14)$$

In Zone 2: $$\frac{\partial^2 \Omega_2}{\partial x^2} - K\,\Omega_2 = \frac{\partial T}{\partial x} \qquad \ldots\ldots (15)$$

$$T = \frac{j\,\omega\,\mu_0\mu_r}{(\rho K + j\,\omega\,\mu_0\mu_r)}\,\frac{\partial \Omega_2}{\partial x} \qquad \ldots\ldots (16)$$

If Eqn. (16) is differentiated with respect to x and substituted into Eqn. (15), the final differential form is:

$$\frac{\partial^2 \Omega_2}{\partial x^2} - \left\{K + \frac{j\,\omega\,\mu_0\mu_r}{\rho}\right\}\Omega_2 = 0 \qquad \ldots\ldots (17)$$

The boundary conditions are:

At $x = 0$ (stator surface):

$$\Omega_1 = \Omega_m \quad \text{(surface value)}$$

At $x = x_1$ (interface between air-gap and rotor), tangential H and normal B are continuous, i.e.

$$\Omega_1 = \Omega_2$$

and $$-\frac{\partial \Omega_1}{\partial x} = \mu_r\left\{T - \frac{\partial \Omega_2}{\partial x}\right\}$$

At $x = x_2$:

$$\Omega_2 = 0 \quad \text{(no tangential flux density)}$$

Solving Eqns. (13) and (17) leads to:

$$\Omega_1 = \Omega_m\left[\frac{\sinh t(x_1 - x_2)\cosh s(x_1 - x) - M\cosh t(x_1 - x_2)\sinh s(x_1 - x)}{\sinh t(x_1 - x_2)\cosh s x_1 - M\cosh t(x_1 - x_2)\sinh s x_1}\right] \qquad \ldots\ldots (18)$$

$$\Omega_2 = \frac{-\Omega_m \sinh t(x_2 - x)}{\{\sinh t(x_1 - x_2)\cosh s x_1 - M\cosh t(x_1 - x_2)\sinh s x_1\}} \qquad \ldots\ldots (19)$$

where: $$s = \frac{\pi}{2lh}\,(h^2 + l^2)^{\frac{1}{2}}$$

$$t = \left\{\frac{\pi^2}{4l^2} + \frac{\pi^2}{4h^2} + \frac{j\,\omega\,\mu_0\mu_r}{\rho}\right\}^{\frac{1}{2}}$$

$$M = \mu_r\,\frac{s}{t}$$

T is obtained by substituting Eqn. (19) into Eqn. (16):

$$T = \frac{j\,\omega\,\mu_0\mu_r\,t\,\Omega_m}{(\rho K + j\,\omega\,\mu_0\mu_r)} \times \left\{\frac{\cosh t(x_2 - x)}{\sinh t(x_1 - x_2)\cosh s x_1 - M\cosh t(x_1 - x_2)\sinh s x_1}\right\} \qquad \ldots\ldots (20)$$

Eqns. (18) - (20) are used when checking the validity of the finite-element numerical equations.

3.3 Numerical Solution

The differential equations which have to be formulated numerically when all the assumptions have been included are:

Zone 1 (non-conducting regions):

$$\frac{\partial^2 \Omega}{\partial x^2} - K\,\Omega = 0 \qquad \ldots\ldots (21)$$

Zone 2 (conducting regions):

$$\mu_0\mu_r\,\frac{\partial^2 \Omega}{\partial x^2} - \mu_0\mu_r\,K\,\Omega = \mu_0\mu_r\,\frac{\partial T}{\partial x} \qquad \ldots\ldots (22)$$

and $$\left\{1 - \frac{j\,\rho\,K}{\omega\,\mu_0\mu_r}\right\}T = \frac{\partial \Omega}{\partial x} \qquad \ldots\ldots (23)$$

To represent the above equations in variational form, an integral equation is formed which, when operated upon by Euler's equation, reverts back to the original differential equation. (A practical way of defining the integral is to establish the energy of the system.)

Thus the functional for the above equations is:

Zone 1:

$$\chi_\Omega = \frac{\mu_0}{2}\int\left\{\frac{\partial \Omega}{\partial x}\right\}^2 dx + \frac{\mu_0 K}{2}\int \Omega^2\,dx$$

Zone 2:

$$\chi_\Omega = \frac{\mu_0\mu_r}{2}\int\left\{\frac{\partial \Omega}{\partial x}\right\}^2 dx + \frac{\mu_0\mu_r K}{2}\int \Omega^2\,dx + \mu_0\mu_r\int \Omega\,\frac{\partial T}{\partial x}\,dx$$

$$\chi_T = \left\{1 - \frac{j\,\rho\,K}{\omega\,\mu_0\mu_r}\right\}\frac{T^2}{2} - \frac{\partial \Omega}{\partial x}\,T$$

The final minimised form is obtained by differentiating with respect to the unknown potential, Ω or T, keeping the other variable constant, and equating to zero, i.e.:

$$\frac{\partial \chi_\Omega}{\partial \Omega_i} = \mu_0\mu_r\int\frac{\partial}{\partial \Omega_i}\left\{\frac{\partial \Omega}{\partial x}\right\}\frac{\partial \Omega}{\partial x}\,dx + \mu_0\mu_r K\int \Omega\,\frac{\partial \Omega}{\partial \Omega_i}\,dx + \mu_0\mu_r\,\frac{\partial T}{\partial x}\int\frac{\partial \Omega}{\partial \Omega_i}\,dx = 0 \qquad \ldots\ldots (24)$$

(For Zone 1 equation, the last term vanishes)

$$\frac{\partial \chi_T}{\partial T_i} = \left\{ 1 - \frac{j \rho K}{\omega \mu_o \mu_r} \right\} T_i - \frac{\partial \Omega}{\partial x}$$

$$= 0 \qquad \ldots\ldots\ldots (25)$$

where Ω_i and T_i are potentials at node i in the region considered.

The element used to represent numerically the potential variation is a "line" element, with a linear distribution between nodes. Thus the numerical equations become:

Zone 1:

$$\frac{\mu_o \mu_r}{3L} (3 + K L^2) \Omega_i + \frac{\mu_o \mu_r}{6L} (-6 + K L^2) \Omega_j = 0 \qquad \ldots\ldots (26)$$

Zone 2:

$$\frac{\mu_o \mu_r}{3L} (3 + K L^2) \Omega_i + \frac{\mu_o \mu_r}{6L} (-6 + K L^2) \Omega_j - \frac{(T_i - T_j)}{2} \mu_o \mu_r = 0$$

$$\ldots\ldots\ldots (27)$$

$$\left\{ 1 - \frac{j \rho K}{\omega \mu_o \mu_r} \right\} T_i + \frac{(\Omega_a - \Omega_b)}{(l_a + l_b)} = 0 \qquad \ldots\ldots\ldots (28)$$

where: Ω_a - scalar potential above node i
Ω_b - scalar potential below node i
L - length of element
l_a, l_b - distance between nodes a and i and b and i respectively

Eqns. (26) - (28) are used to obtain the potential distribution in all the configurations used in the test cases, together with the boundary equations described in the following section.

3.4 Boundary Equations

The equations derived in the previous section only apply within the relevant regions, and not at the interfaces between them. The conditions to be obeyed at interfaces between non-conducting and conducting regions are:

$H_{tangential}$ is continuous

B_{normal} is continuous

J_{normal} is zero

The last is automatically satisfied by assuming only one value of T at the interface (T_{normal}).

Continuity of tangential H is automatically satisfied in the single T - Ω solution, since Ω is common to both regions,

i.e. $H_{y1} = H_{y2} = -\frac{\partial \Omega}{\partial y}$

and $H_{z1} = H_{z2} = -\frac{\partial \Omega}{\partial z}$

The continuity of normal B condition is more difficult, since its value relies on Ω in the non-conducting region, and on T and Ω in the conducting region. This can be overcome by rewriting Eqn. (10) as:

$$\left\{ \frac{\partial^2 T}{\partial y^2} + \frac{\partial^2 T}{\partial z^2} \right\} = j \omega B_T$$

Now B_T can be written in any one of the following ways:-

$$B_x = -\mu_o \frac{\partial \Omega}{\partial x} \qquad \text{(based on air values)}$$

$$B_x = \mu_o \mu_r \left\{ T - \frac{\partial \Omega}{\partial x} \right\} \qquad \text{(based on rotor values)}$$

$$B_T = \frac{\mu_o}{2} \left[\mu_r \left\{ T - \frac{\partial \Omega}{\partial x} \right\} - \frac{\partial \Omega}{\partial x} \right] \qquad \left[\text{based on the average of the air and rotor flux densities} \right]$$

All three conditions have been incorporated in the variational equations.

It is also necessary to allow for the contribution to the scalar potential equation arising from the discontinuity in T at the interface.

The term $\partial T/\partial x$ in Eqn. (24) can be evaluated at the discontinuity as:

$$\mu_o \mu_r \int_{x_{1-}}^{x_{1+}} \frac{\partial T}{\partial x} dx = \mu_o \mu_r \{ T(x_{1+}) - T(x_{1-}) \}$$

$$= \mu_o \mu_r T_i$$

This modifies Eqn. (27) at the interface only.

The other boundary conditions, i.e. $\Omega = T$ = value and $\partial \Omega/\partial n = \partial T/\partial n = 0$, are automatically satisfied by the variational formulation.

4. RESULTS FROM TEST PROBLEMS

To determine the most suitable interface condition, and the effect of different discretisations on the accuracy of the numerical solution, the following studies were made for the geometry of Fig. 1:-

(a) Copper rotor: $\mu_r = 1$ and $\rho = 2 \times 10^{-8} \Omega$-m

(b) Mild steel rotor: $\mu_r = 100$ and $\rho = 16 \times 10^{-8} \Omega$-m

The effect of discretisation is shown in Figs. 3 and 4, and Fig. 5 compares the effect of the different interface conditions used.

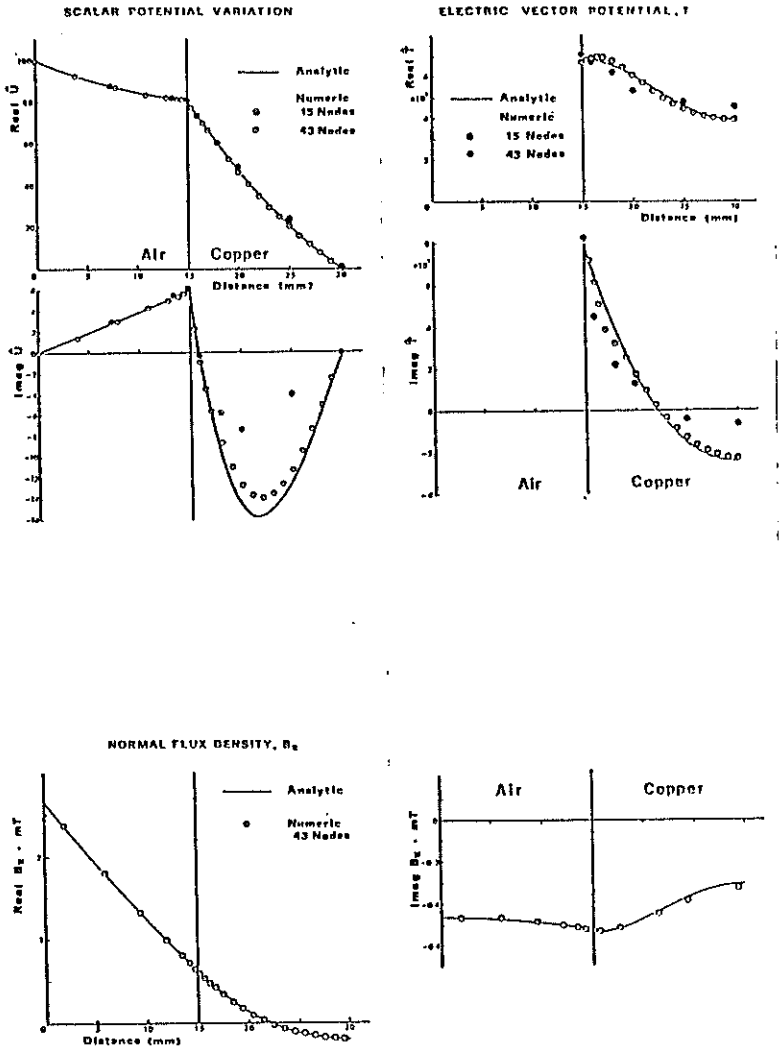

Fig. 3: Copper rotor - Effect of discretisation

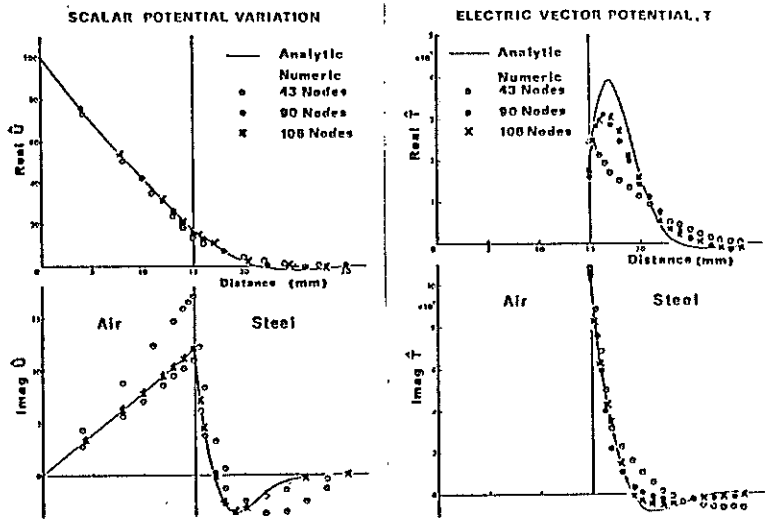

Fig. 4: Steel rotor - Effect of discretisation

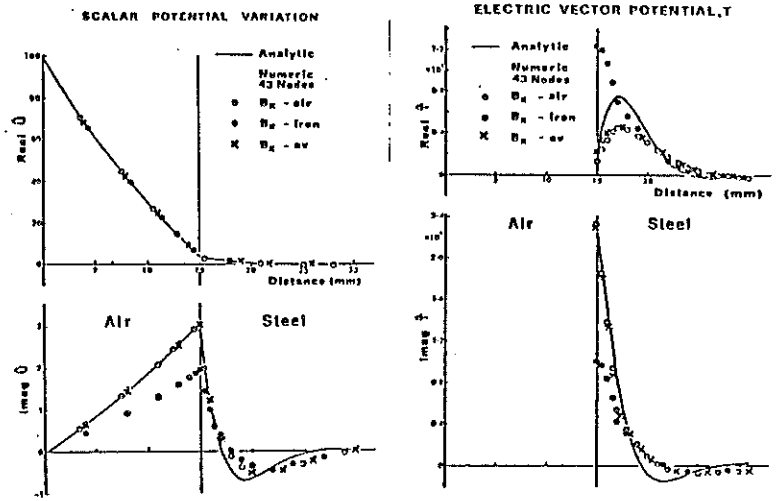

Fig. 5: Steel rotor - Effect of interface conditions

The results show that:

(i) Fine discretisation is essential in a magnetic member to obtain close agreement with the analytic results. This is associated with the thin skin depth, viz. 2 mm, compared with 7 mm for the copper rotor. A possible way in which this problem could be overcome is to represent thin skin materials by impedance sheets as described in Ref. 4.

(ii) The best interface condition to use is the one in which the normal flux density is based on the air values, since this is less sensitive to discretisation changes.

The work described has shown that a variational approach can be used to obtain the T - Ω solution for eddy current problems. The following section describes the formulation of the "single T" - Ω equations for the full 3-dimensional problem, i.e. with no reduction in the number of dimensions through assumed analytic variations.

5. FULL 3-DIMENSIONAL NUMERICAL EQUATIONS

The functional for the full 3-dimensional magnetic scalar potential equation (Eqn. (9)) can be obtained by using the restricted variations technique, in this case keeping T constant.

$$\chi_\Omega = \frac{\mu}{2}\int_V \left[\left\{\frac{\partial\Omega}{\partial x}\right\}^2 + \left\{\frac{\partial\Omega}{\partial y}\right\}^2 + \left\{\frac{\partial\Omega}{\partial z}\right\}^2\right] dV + \mu\frac{\partial T}{\partial x}\int_V \Omega\, dV$$

In non-conducting regions:

$$\mu\frac{\partial T}{\partial x}\int \Omega\, dV = 0$$

The minimised form of the above equation is:

$$\frac{\partial\chi_\Omega}{\partial\Omega_i} = \mu\int_V\left[\frac{\partial}{\partial\Omega_i}\left\{\frac{\partial\Omega}{\partial x}\right\}\frac{\partial\Omega}{\partial x} + \frac{\partial}{\partial\Omega_i}\left\{\frac{\partial\Omega}{\partial y}\right\}\frac{\partial\Omega}{\partial y} + \frac{\partial}{\partial\Omega_i}\left\{\frac{\partial\Omega}{\partial z}\right\}\frac{\partial\Omega}{\partial z}\right]dV + \mu\frac{\partial T}{\partial x}\int_V\frac{\partial\Omega}{\partial\Omega_i}dV$$

$$= 0 \qquad \ldots\ldots\ (29)$$

$$\chi_T = \frac{\rho}{2}\int_V\left[\left\{\frac{\partial T}{\partial y}\right\}^2 + \left\{\frac{\partial T}{\partial z}\right\}^2\right]dV + \frac{j\,\omega\,\mu}{2}\int_V T^2\, dV - j\,\omega\,\mu\frac{\partial\Omega}{\partial x}\int_V T\, dV$$

Since currents are assumed to flow only in the y-z plane and the distribution of Ω is constant through the restricted variations principle, the minimisation condition for χ_T involves an area integral only.

$$\frac{\partial\chi_T}{\partial T_i} = \rho\int_A\left[\frac{\partial}{\partial T_i}\left\{\frac{\partial T}{\partial y}\right\}\frac{\partial T}{\partial y} + \frac{\partial}{\partial T_i}\left\{\frac{\partial T}{\partial z}\right\}\frac{\partial T}{\partial z}\right]dA + j\,\omega\,\mu\int_A T\frac{\partial T}{\partial T_i}dA$$

$$- j\,\omega\,\mu\frac{\partial\Omega}{\partial x}\int_A\frac{\partial T}{\partial T_i}dA \qquad \ldots\ldots\ (30)$$

If a linear shape function is chosen for Ω and T, the numerical equations for the tetrahedral element become:

Scalar magnetic potential

$$\frac{\mu}{36V}\{(b_i^2 + c_i^2 + d_i^2)\Omega_i + (b_ib_j + c_ic_j + d_id_j)\Omega_j$$

$$+ (b_ib_m + c_ic_m + d_id_m)\Omega_m + (b_ib_p + c_ic_p + d_id_p)\Omega_p\}$$

$$+ \frac{\mu}{24}(b_iT_i + b_jT_j + b_mT_m + b_pT_p) = 0 \qquad \ldots\ldots\ (31)$$

where: b_i, c_i, d_i, etc. are terms related to the x, y and z co-ordinates of the tetrahedron
V = volume of tetrahedron

Electric vector potential

$$\left\{\frac{(b_i^2 + c_i^2)}{4\Delta}\rho + j\,\frac{\omega\,\mu\,\Delta}{6}\right\}T_i + \left\{\frac{(b_ib_j + c_ic_j)}{4\Delta}\rho + j\,\frac{\omega\,\mu\,\Delta}{12}\right\}T_j$$

$$+ \left\{\frac{(b_ib_m + c_ic_m)}{4\Delta}\rho + j\,\frac{\omega\,\mu\,\Delta}{12}\right\}T_m - j\,\frac{\omega\,\mu\,\Delta}{3l_x}(\Omega_u - \Omega_l) = 0 \quad \ldots\ (32)$$

where: Ω_u - scalar potential directly above node i
Ω_l - scalar potential directly below node i
l_x - distance between Ω_u and Ω_l
Δ - area of triangle

The equation for magnetic scalar potential applies throughout, but, as mentioned in Section 3, an extra term is required at the interface to account for the discontinuity in T. This term is:

$$\mu\frac{\Delta T_i}{3}$$

Similarly for the electric vector potential the normal flux density at the interface has to be forced: in this work, the air value alone has been used.

To check the validity of the above equations, the test problems were repeated with the y and z variations treated numerically.

Fig. 1 shows the discretisation used for the copper rotor with y and z pole pitches of 30 mm, and Fig. 6 shows the comparison with analytical values for scalar and electric vector potential respectively.

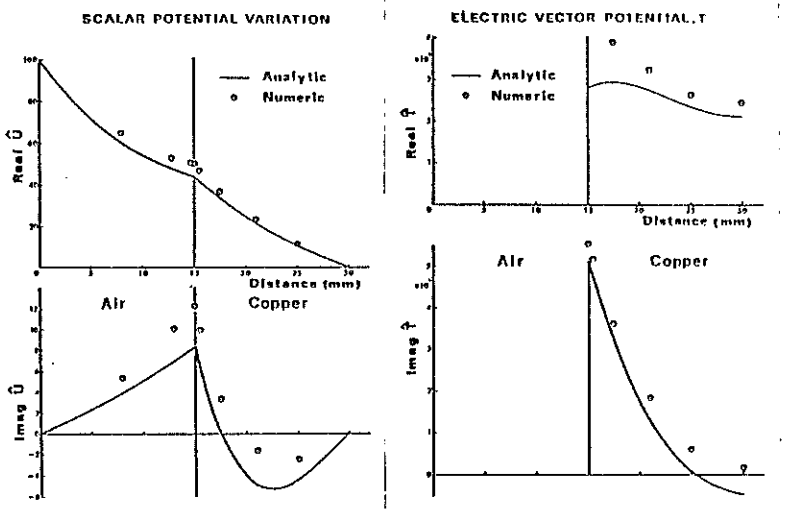

Fig. 6: Copper rotor - 3-dimensional numerical treatment

Agreement is less good than in the 1-dimensional case, but since the discretisation is poor in the y- and z-directions, the result is not too surprising. A more refined mesh is needed, but since the matrix equations were solved by the direct-Gaussian Elimination Method, a large amount of computer storage was required, and computation was costly. An iterative method of solution is probably more appropriate, and is being investigated.

Although restricted in the number of nodes that can be used, an attempt was made to calculate the current flow in and around the junction between slot wedges of a rotor, as shown in Fig. 7.

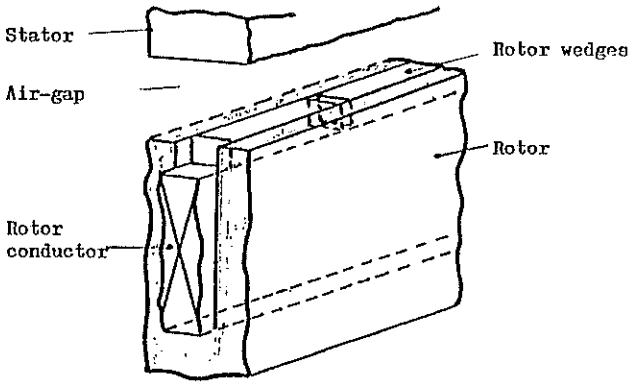

Fig. 7: Rotor wedge problem

The calculated current flow lines (real T values) are given in Fig. 8, and indicate a crowding of current in the rotor iron at the end of the wedge. This figure also shows the variation of the axial current density across the rotor iron section for a continuous wedge and a short wedge.

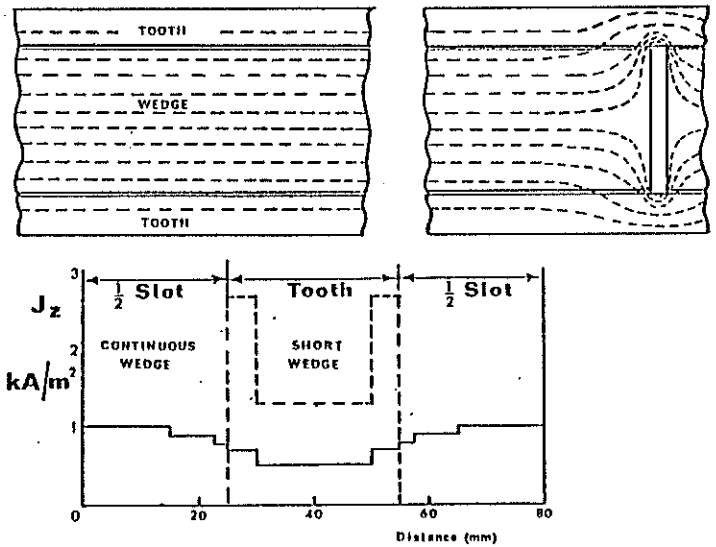

Fig. 8: Rotor wedge problem - Surface current flow and densities

6. "TWO-T" - Ω EQUATIONS

This work is still in its early stages, but, as mentioned in Section 1, only two components of T are required to describe all three components of current density.

The resulting equations for two values of T, i.e. T_x and T_y, are:

$$\mu\left\{\frac{\partial^2\Omega}{\partial x^2}+\frac{\partial^2\Omega}{\partial y^2}+\frac{\partial^2\Omega}{\partial z^2}\right\} = \mu\left\{\frac{\partial T_x}{\partial x}+\frac{\partial T_y}{\partial y}\right\}$$

$$\rho\left\{\frac{\partial^2 T_x}{\partial y^2}+\frac{\partial^2 T_x}{\partial z^2}-\frac{\partial^2 T_y}{\partial x\,\partial y}\right\} = j\,\omega\,\mu\left\{T_x-\frac{\partial\Omega}{\partial x}\right\}$$

$$\rho\left\{\frac{\partial^2 T_y}{\partial x^2}+\frac{\partial^2 T_y}{\partial z^2}-\frac{\partial^2 T_x}{\partial x\,\partial y}\right\} = j\,\omega\,\mu\left\{T_y-\frac{\partial\Omega}{\partial y}\right\}$$

The following minimised functionals can be derived from consideration of the energy equation:-

$$\frac{\partial \chi}{\partial \Omega_i} = -\mu \int_V \left[\frac{\partial}{\partial \Omega_i}\left\{\frac{\partial \Omega}{\partial x}\right\}\frac{\partial \Omega}{\partial x} + \frac{\partial}{\partial \Omega_i}\left\{\frac{\partial \Omega}{\partial y}\right\}\frac{\partial \Omega}{\partial y} + \frac{\partial}{\partial \Omega_i}\left\{\frac{\partial \Omega}{\partial z}\right\}\frac{\partial \Omega}{\partial z} - T_x \frac{\partial}{\partial \Omega_i}\left\{\frac{\partial \Omega}{\partial x}\right\} - T_y \frac{\partial}{\partial \Omega_i}\left\{\frac{\partial \Omega}{\partial y}\right\}\right] dV$$

$$= 0$$

$$\frac{\partial \chi}{\partial T_{x_i}} = -\mu \int_V \left[\left\{ T_x \frac{\partial T_r}{\partial T_{x_i}} - \frac{\partial \Omega}{\partial x}\frac{\partial T_r}{\partial T_{x_i}} \right\} dV + j\frac{\rho}{\omega}\int_V \frac{\partial}{\partial T_{x_i}}\left\{\frac{\partial T_r}{\partial z}\right\}\frac{\partial T_r}{\partial z} + \frac{\partial}{\partial T_{x_i}}\left\{\frac{\partial T_r}{\partial y}\right\}\frac{\partial T_r}{\partial y} - \frac{\partial T_u}{\partial x}\frac{\partial}{\partial T_{x_i}}\left\{\frac{\partial T_r}{\partial y}\right\}\right] dV$$

$$= 0$$

$$\frac{\partial \chi}{\partial T_{y_i}} = -\mu \int_V \left\{ T_u \frac{\partial T_u}{\partial T_{y_i}} - \frac{\partial \Omega}{\partial y}\frac{\partial T_u}{\partial T_{y_i}} \right\} dV + j\frac{\rho}{\omega}\int_V \left[\frac{\partial}{\partial T_{y_i}}\left\{\frac{\partial T_u}{\partial z}\right\}\frac{\partial T_u}{\partial z} + \frac{\partial}{\partial T_{y_i}}\left\{\frac{\partial T_u}{\partial x}\right\}\left\{\frac{\partial T_u}{\partial x}\right\} - \frac{\partial T_x}{\partial y}\frac{\partial}{\partial T_{y_i}}\left\{\frac{\partial T_u}{\partial x}\right\}\right] dV$$

$$= 0$$

It was intended to show the application of the "two-T" - Ω approach, but, because direct matrix inversion has been used, the cost for a realistic discretisation was high. Attention is therefore now being aimed at development of an iterative solution in order to reduce the computation costs, and to enable non-linear materials to be represented efficiently.

7. CONCLUSIONS

Although still in its early stages, the indications are that the finite-element formulation of the T - Ω method can be used to solve full 3-dimensional eddy current problems.

However, the finite-element formulation loses some of its normally accepted advantages: in particular, all interface conditions have to be met. Not surprisingly, 3-dimensional solutions raise the problem of computer costs, and it is uneconomical to represent materials with thin skin depths, such as the rotor iron, by the T formulation, because of the need to discretise finely. An impedance-sheet representation should avoid this problem.

For large 3-dimensional problems, iterative solution is required to make the method economically feasible.

8. ACKNOWLEDGMENTS

The authors thank Mr. C.J. Carpenter for his advice and encouragement, and G.E.C. Power Engineering Ltd. for permission to publish.

9. REFERENCES

1. Carpenter, C.J., and Wyatt, E.A.,
"Efficiency of numerical techniques for computing eddy currents in two and three dimensions",
Compumag 1976, pp. 242-250.

2. Carpenter, C.J.,
"Comparison of alternative formulations of 3-dimensional magnetic-field and eddy-current problems at power frequencies",
Proc. I.E.E., 1977, 124(11), pp. 1026-1034.

3. Wolff, W.,
"Three dimensional eddy current calculations",
Compumag 1976, pp. 231-241.

4. Preston, T.W., and Reece, A.B.J.,
"The prediction of machine end-region fluxes, allowing for eddy current losses in thick components",
Compumag 1976, pp. 213-220.

COMPUTATION OF TRANSIENT 3-D EDDY CURRENT IN NONMAGNETIC CONDUCTOR*

H. T. Yeh
Oak Ridge National Laboratory, Oak Ridge, Tennessee 37830, USA

ABSTRACT

A numerical procedure was developed to solve transient three-dimensional (3-D) eddy current problems for nonmagnetic conductor. Integral equation formulation in terms of vector potential is used to simplify the matching of boundary conditions. The resulting equations and their numerical approximation were shown to be singular and to require special handling. Several types of symmetries were introduced. They not only reduce the number of algebraic equations to be solved, but also modify the nature of the equations and render them nonsingular. Temporal behavior was obtained with the Runge-Kutta method. The program is tested in several examples of eddy currents for its spatial and temporal profiles, shielding, boundary surface effects, and application of various symmetry options.

1. INTRODUCTION

In tokamak-type fusion devices, pulsed magnetic fields are required and 3-D transient eddy currents are produced. A code is needed to compute these eddy currents. A finite difference method is not easy to implement for such a system due to geometrical complexity (e.g., toroidal field coils may have noncircular shapes). Boundary conditions are easier to handle with the field equations formulated as integral equations. The vector potential $\underline{A}$ fits naturally with these requirements and has been adopted as the basic variable in earlier work. A Coulomb gage is appropriate for this application, and our code for the external vector potential $\underline{A}_o$ is formulated in this gage.[1] This choice implied that the scalar potential ϕ is needed to describe the effect of surface charges, which are induced by the interruption of eddy current at the boundary.

Previously, we tried to solve the time-dependent part of the field equation by a perturbation-polynomial expansion method.[1,2] Although this approach exhibits no stability problem, it is not suitable when shielding becomes significant, i.e., if the skin time of the conductor is longer than the characteristic time of the pulse. A different approach has been used successfully on 2-D transient eddy current problems by Biddlecombe et al.[3] In this paper, their approach has been adopted, with some modifications, for the 3-D problem. As before, we limit ourselves to a single nonmagnetic conductor with constant conductivity. The external source is assumed to have a given current waveform, and the interactions between eddies of different conductors are assumed to be small and negligible.

Our basic equations, as derived earlier,[1,3] are summarized below (SI units are used):

$$\underline{A}(\underline{r},t) = \underline{A}_o(\underline{r},t) - \frac{\mu_o\sigma}{4\pi}\int \frac{(\partial\underline{A}/\partial t) + \nabla\phi}{|\underline{r}-\underline{r}'|}\, d^3r' \,, \tag{1}$$

$$\phi(\underline{r},t) = -\frac{1}{2\pi}\oint \left[\frac{(\partial\underline{A}/\partial t)}{|\underline{r}-\underline{r}'|} + \phi\nabla'\left(\frac{1}{|\underline{r}-\underline{r}'|}\right)\right]\cdot d\underline{S}' \,. \tag{2}$$

Here, the integration is over the conductor volume and surface, respectively, and σ is the conductivity. In Eq. (2), the factor 2π is used when $\underline{r}$ lies on the boundary surface. For interior points, it should be replaced by 4π.

2. NUMERICAL DISCRETIZATION

The conductor volume is divided into N 8-node bricks, and the boundary surface into L quadrilateral surfaces. For simplicity, $(\partial\underline{A}/\partial t)$ and $\nabla\phi$ are assumed to be constant over each volume element, and ϕ is assumed to be constant over each boundary surface element. After discretization, Eqs. (1) and (2) become

$$\underline{A}_i = \underline{A}_{oi} + \sum_{j=1}^{N} R_{ij}\left[\frac{d\underline{A}_j}{dt} + (\nabla\phi)_j\right] \,, \tag{3}$$

$$\frac{1}{2}\phi_\ell = \sum_{k=1}^{L}\left[\Omega_{\ell k}\phi_k + U_{\ell k}\left(\frac{dA_n}{dt}\right)_k\right] \,. \tag{4}$$

In Eq. (4) the factor 1/2 is replaced by 1 for interior points. The expression $(dA_n/dt)_k$ is the rate of change of the outward normal component of $\underline{A}$ in the volume element where the kth boundary surface element belongs. Coefficients are defined by

$$R_{ij} = -\frac{\mu_o\sigma}{4\pi}\int \frac{d^3r_j}{|\underline{r}_i - \underline{r}_j|} \,, \tag{5}$$

$$\Omega_{\ell k} = -\frac{1}{4\pi}\int \frac{\partial}{\partial n}\frac{1}{|\underline{r}_\ell - \underline{r}_k|}\, dS_k \,, \tag{6}$$

$$U_{\ell k} = -\frac{1}{4\pi}\int \frac{dS_k}{|\underline{r}_\ell - \underline{r}_k|} \,. \tag{7}$$

Collie[4] derived formulas to reduce integration over volume to integration over surface and line, and $i = j$ or $\ell = k$ cases do not present special difficulties.

It was noted earlier[2,5] that Eq. (2) was "singular" in the operator sense. This singularity is preserved in Eq. (4),

* Research sponsored by the Office of Fusion Energy (ETM), U.S. Department of Energy under Contract No. W-7405-eng-26 with Union Carbide Corporation.

provided that the coefficients in Eqs. (5)-(7) are evaluated exactly. If crude approximations to Eq. (6) were used, examples showed that the numerical result converges to the wrong answer in an iterated solution.[6]

In general, subdivision into volume and surface elements of equal sides tends to give better numerical results. In particular, for a thin, flat, platelike conductor, the terms on the right-hand side of Eq. (4) are dominated by the solid angles $\Omega_{\ell k}$ associated with the top and bottom surfaces of the plate. These terms change very slowly for points around the centroid of the element. Hence, the direct differentiation of Eq. (4) may not reflect the actual variation of ϕ across the element. Instead, we approximate $(\nabla\phi)_j$ of Eq. (3) as the vector sum of the central difference of ϕ, between opposing surface centroids. This approximation becomes less accurate for more highly askew volume elements.

3. ELIMINATION OF $\nabla\phi$

To eliminate $(\nabla\phi)_j$ in Eq. (3), we first solve for ϕ_ℓ's on the boundary surfaces by Eq. (4). Since this equation is singular,

$$\sum_{k=1}^{L} \Omega_{\ell k} = \frac{1}{2} ,$$

the ϕ_ℓ obtained will be of large magnitude (if no overflow error occurs during computer operation). The $(\nabla\phi)_j$ which results from subtracting two large ϕ's may have substantial error. This singularity is related to the fact that only $\nabla\phi$ is prescribed at the boundary surface; hence, ϕ is not determined to within a constant. This uncertainty can be removed by fixing the ϕ value of one of the boundary surface elements at zero. $\nabla\phi$ was found to be insensitive to which value of ϕ_ℓ was chosen to be zero.

Next, the scalar potential is computed for the centroids of the surfaces of each volume element by Eq. (4). $(\nabla\phi)_j$ is then obtained as the central difference. Let $\underline{X2}$, $\underline{X1}$; $\underline{Y2}$, $\underline{Y1}$; and $\underline{Z2}$, $\underline{Z1}$ represent the position vectors to centroids of opposing faces. Then

$$(\nabla\phi) = \frac{\phi_{X2} - \phi_{X1}}{|\underline{X2} - \underline{X1}|^2} (\underline{X2} - \underline{X1}) + \frac{\phi_{Y2} - \phi_{Y1}}{|\underline{Y2} - \underline{Y1}|^2} (\underline{Y2} - \underline{Y1}) + \frac{\phi_{Z2} - \phi_{Z1}}{|\underline{Z2} - \underline{Z1}|^2} (\underline{Z2} - \underline{Z1}). \tag{8}$$

After elimination, we have

$$A_{ix} - A_{oix} = \sum_{j=1}^{N} \left(M_{ij}^{xx} \frac{dA_{jx}}{dt} + M_{ij}^{xy} \frac{dA_{jy}}{dt} + M_{ij}^{xz} \frac{dA_{jz}}{dt} \right) , \tag{9a}$$

$$A_{iy} - A_{oiy} = \sum_{j=1}^{N} \left(M_{ij}^{yx} \frac{dA_{jx}}{dt} + M_{ij}^{yy} \frac{dA_{jy}}{dt} + M_{ij}^{yz} \frac{dA_{jz}}{dt} \right) , \tag{9b}$$

$$A_{iz} - A_{oiz} = \sum_{j=1}^{N} \left(M_{ij}^{zx} \frac{dA_{jx}}{dt} + M_{ij}^{zy} \frac{dA_{jy}}{dt} + M_{ij}^{zz} \frac{dA_{jz}}{dt} \right) , \tag{9c}$$

where

$$M_{ij}^{xx} = R_{ij} + \sum_{p=1}^{N} R_{ip} \sum_{t=1}^{6} \Delta_{tj} (Fx)_{p,tj} \hat{S}_{tj,x} , \tag{10a}$$

$$M_{ij}^{xy} = \sum_{p=1}^{N} R_{ip} \sum_{t=1}^{6} \Delta_{tj} (Fx)_{p,tj} \hat{S}_{tj,y} , \tag{10b}$$

$$M_{ij}^{xz} = \sum_{p=1}^{N} R_{ip} \sum_{t=1}^{6} \Delta_{tj} (Fx)_{p,tj} \hat{S}_{tj,z} , \tag{10c}$$

$$M_{ij}^{yx} = \sum_{p=1}^{N} R_{ip} \sum_{t=1}^{6} \Delta_{tj} (Fy)_{p,tj} \hat{S}_{tj,x} , \tag{10d}$$

$$M_{ij}^{yy} = R_{ij} + \sum_{p=1}^{N} R_{ip} \sum_{t=1}^{6} \Delta_{tj} (Fy)_{p,tj} \hat{S}_{tj,y} , \tag{10e}$$

$$M_{ij}^{yz} = \sum_{p=1}^{N} R_{ip} \sum_{t=1}^{6} \Delta_{tj} (Fy)_{p,tj} \hat{S}_{tj,z} , \tag{10f}$$

$$M_{ij}^{zx} = \sum_{p=1}^{N} R_{ip} \sum_{t=1}^{6} \Delta_{tj} (Fz)_{p,tj} \hat{S}_{tj,x} , \tag{10g}$$

$$M_{ij}^{zy} = \sum_{p=1}^{N} R_{ip} \sum_{t=1}^{6} \Delta_{tj} (Fz)_{p,tj} \hat{S}_{tj,y} , \tag{10h}$$

$$M_{ij}^{zz} = R_{ij} + \sum_{p=1}^{N} R_{ip} \sum_{t=1}^{6} \Delta_{tj} (Fz)_{p,tj} \hat{S}_{tj,z} , \tag{10i}$$

The Fx, Fy, and Fz matrices are defined by Eqs. (3) and (8), and

$$(\nabla\phi)_{jx} = \sum_{k=1}^{L} (Fx)_{jk}\left(\hat{S}_k \cdot \frac{d\underline{\Lambda}_k}{dt}\right), \tag{11a}$$

$$(\nabla\phi)_{jy} = \sum_{r=1}^{L} (Fy)_{jk}\left(\hat{S}_k \cdot \frac{d\underline{\Lambda}_k}{dt}\right), \tag{11b}$$

$$(\nabla\phi)_{jz} = \sum_{k=1}^{L} (Fz)_{jk}\left(\hat{S}_k \cdot \frac{d\underline{\Lambda}_k}{dt}\right). \tag{11c}$$

$\hat{S}$ is the unit outward normal vector on the boundary surface. The sum over boundary surface elements,

$$\sum_{k=1}^{L},$$

may be converted into a sum over volume elements,

$$\sum_{k=1}^{L} \rightarrow \sum_{p=1}^{N} \sum_{t=1}^{6} \Delta_{tj}, \tag{12}$$

with

$$\sum_{t=1}^{6}$$

the sum over all the surfaces of a volume element and $\Delta_{tj} = 0$ if it is not a boundary surface and $\Delta_{tj} = 1$ if it is a boundary surface.

Equation (9) is solved, after direct matrix inversion, by the Runge-Kutta method. Then the eddy current in volume element i is given by

$$\underline{J}_i = -\sigma\left[\frac{d\underline{\Lambda}_i}{dt} + (\nabla\phi)_i\right]. \tag{13}$$

The eigenvalues of the M-matrix of Eq. (10) have been checked. Eigenvalues with a positive real part, implying growing rather than decaying transients, were sometimes encountered, but only for conductors using very coarse meshes (one or two volume elements). For finer meshes, the real part of eigenvalues seems to be always negative and insensitive to the choice of which surface element scalar potential is set to be zero.

4. SYMMETRY CONSIDERATION

Since the M-matrix of Eq. (10) is dense and needs direct inversion, its dimension should be minimized. This can be done if the conductor and source currents possess certain symmetries, so knowledge of the resulting eddy current in one part of the conductor implies knowledge of those of other parts. Certain types of symmetries, furthermore, remove the singular character of the equation. The following two properties of Maxwell's equation are the basis of our symmetry consideration.

(a) Maxwell's equation is invariant under reflection transformation. Hence, for a conductor with reflection symmetry, if the source currents are reflected, so are the induced currents.

(b) Maxwell's equation is linear. Thus, if the source currents are reversed, so are the induced eddy currents.

Four types of symmetries are now considered.

4.1 Reflection symmetry (Type 1)

Assume that the source current $\underline{J}_o$ and the conductor are invariant under reflection transformation about the x-z plane. That is, for given x,z,

$$J_{ox}(y) = J_{ox}(-y),\ J_{oy}(y) = -J_{oy}(-y),\ J_{oz}(y) = J_{oz}(-y). \tag{14}$$

Then, from property (a) above, we expect that the induced eddy current $\underline{J}$ also transforms like Eq. (14). The symmetric nature of R_{ij} also implies that $\underline{\Lambda}$ (and hence $d\underline{\Lambda}/dt$) transforms like Eq. (14). Hence $(\partial\phi/\partial n)(y) = (\partial\phi/\partial n)(-y)$, $\phi(y) = \phi(-y)$, and $\nabla\phi$ also transform like Eq. (14). Although this symmetry allows us to reduce the order of the M-matrix by half, the resulting equations remain singular in nature.

4.2 Reflection symmetry plus current reversion (Type 2)

Assume that the conductor is invariant under reflection transformation about the x-z plane, but the source current $\underline{J}_o$ transforms like

$$J_{ox}(y) = -J_{ox}(-y),\ J_{oy}(y) = +J_{oy}(-y),\ J_{oz}(y) = -J_{oz}(-y), \tag{15}$$

that is, reflection plus reversion. From properties (a) and (b), one can show that $\underline{J}$, $\underline{\Lambda}$, $d\underline{\Lambda}/dt$, and $\nabla\phi$ also transform like Eq. (15), and $\partial\phi/\partial n(y) = -\partial\phi/\partial n(-y)$ and $\phi(-y) + \phi(y) = \text{constant}$.

The reduced matrix equation is not singular. Hence, in solving the reduced equations, the value of ϕ should not be fixed for any boundary surface element. An alternative way to solve ϕ is to apply Eq. (2) to only half of the conductor ($j \geq 0$) with ϕ fixed as some constant in the x-z plane. It then becomes a mixed boundary condition problem, and Eq. (2) is also no longer singular. However, unless sufficient mesh division is provided in the x-z plane, this approach may be less accurate than solving the reduced M-matrix equation.

4.3 Double reflection/reversion symmetry (Type 3)

Assume that conductor and source current satisfies the symmetry described in Sect. 4.2 above for both the x-z plane and the y-z plane (e.g., a square plate in the x-y plane coaxial with a solenoid along the z-axis). Then the induced eddies satisfy (for given z)

$$J_x(x,y) = -J_x(x,-y) = J_x(-x,y) = -J_x(-x,-y),$$

$$J_y(x,y) = J_y(x,-y) = -J_y(-x,y) = -J_y(-x,-y), \quad (16)$$

$$J_z(x,y) = -J_z(x,-y) = -J_z(-x,y) = J_z(-x,-y).$$

4.4 Symmetry for toroidal field (TF) coil in tokamak (Type 4)

Toroidal field (TF) coils and pulse coils in tokamaks possess reflection symmetry (Type 1) about the torus midplane (x-z), and reflection/reversion symmetry (Type 2) about the coil midplane (y-z). Here the induced eddies satisfy

$$J_x(x,y) = J_x(x,-y) = J_x(-x,y) = J_x(-x,-y),$$

$$J_y(x,y) = -J_y(x,-y) = -J_y(-x,y) = J_y(-x,-y), \quad (17)$$

$$J_z(x,y) = J_z(x,-y) = -J_z(-x,y) = -J_z(-x,-y).$$

Both Type 3 and Type 4 symmetries reduce the M-matrix order by a factor of four, and the reduced matrix equations are nonsingular. These symmetry relations have been verified in test examples.

5. EXAMPLES

The 3-D eddy code is structured as a set of four linked programs: mesh generation;[7] computation of matrix coefficients; its inverse, computation of external vector potential; and eddy current calculation. The program is run on a PDP-10 (KL-10). Most CPU time was used for matrix coefficient computation and inversion. This structure allows for changing relative coil/conductor position or pulse waveform without the need to recompute the coefficient matrix. Symmetries are selected as options in the matrix coefficients program.

Small jobs can be run in time-sharing mode. Example 4 below used 24 volume elements and requires 7 minutes of CPU time to compute the matrix elements and inversion, compared to 76 minutes for a batch job of 81 elements (a matrix of order 243).

5.1 Time profile of eddy in a circular ring

A very small coil along the z-axis ramps up linearly and induces eddy current in a coaxial circular ring-shaped conductor. One quarter of the conductor is modeled as eight elements (Type 3 symmetry), as shown in Fig. 1. J_s is the magnitude of the saturated eddy current density and varies about 1% for elements of the same layer. The time profile of the eddy is plotted in Fig. 1. The same problem is also solved by circuit analysis, treating the conductor as two single-turn lumped circuits. The lumped circuit solution agrees with those of Fig. 1 within 3%.

5.2 Spatial profile of eddy in a square plate

A very small coil ramps up linearly and induces eddy current in a 2-m^2 plate, 0.5 m thick. One quarter of the plate was modeled by 25 elements (Type 3 symmetry). The initial (t = 0.1 sec) and the saturated (t = 2 sec) magnitudes of eddy current density J for elements along the line connecting the center of the plate to the center of one side are plotted in Fig. 2, normalized to J_M, the current density of the middle element at that time. Also plotted for comparison is the lumped circuit solution of a circular plate 1 m in diameter. Results are similar to those obtained from previous work.[1] The saturated value of J_M obtained from the 3-D code agrees with the lumped circuit solution within 5%.

5.3 Shielding of an oscillating dipole by a square plate

The dipole and square plate used in example 2 were also used to study the shielding phenomena. Dipole current is assumed to oscillate at 60 Hz. For a plate of infinite area with oscillating current parallel to the surface, the induced eddy decays exponentially. In this example, the skin depth is 8 cm. For a 5-element approximation (each layer 10 cm thick), the logarithmic plot of J(n)/J(n=1), where n is the layer number, has a slope of -1.25. This is represented by the solid line in Fig. 3. Our solution (dotted line) gives exponential decay shielding behavior over three skin depths, and levels off after that. The short solid line (improved solution) corresponds to a 20-element, 5-layer solution, so that the width of each element is now reduced to 50 cm instead of 1 m. This improvement indicates that the time increment and mesh size should be selected to match or be smaller than the characteristic pulse duration and the skin depth, respectively.

5.4 Tokamak symmetry example

A 1-m^2 rectangular plate 0.4 m thick lies in the x-z plane. A linear ramp of source current along the x-axis simulates plasma buildup. One quarter of the plate (Type 4 symmetry) was modeled by 24 elements. The saturated eddy current is plotted in Fig. 4. Eddy current in elements near the x-axis flows opposite to the source current, and the overall eddy forms closed loops in the plate. A shielding current (one order of magnitude smaller) was also created in the x-y plane. Thus, in 3-D examples, eddies perpendicular to the plane of source current are usually created due to boundary and surface charge effects.[2]

ACKNOWLEDGEMENTS

I wish to thank my colleagues W.C.T. Stoddart for making his 3-D mesh generator code available to me and W. H. Gray and K. H. Carpenter for reviewing the manuscript and making helpful comments.

REFERENCES

1. Yeh, H. T. A Perturbation-Polynomial Expansion Formulation of 3-D Eddy Current Problems. Proc. 7th Symp. on Engineering Problems of Fusion Research, p. 1381, Knoxville, Tennessee, October 1977.

2. Carpenter, K. H. and Yeh, H. T. A Perturbation Expansion with Separated Time Dependence for Eddy Current Calculations. Proc. COMPUMAG Conference on the Computation of Magnetic Fields, p. 373, Oxford, April 1976.

3. Biddlecombe, C. S., Collie, C. J., Simkin, J., and Trowbridge, C. W. The Integral Equation Method Applied to Eddy Currents. Proc. COMPUMAG Conf. on the Computation of Magnetic Fields, p. 363, Oxford, April 1976.

4. Collie, C. J. Magnetic Fields and Potential of Linearly Varying Current on Magnetization in a Plane Bounded Region. Proc. COMPUMAG Conf. on the Computation of Magnetic Fields, Oxford, April 1976.

5. Lynn, M. S. and Timlake, W. P. The Numerical Solution of Singular Integral Equations of Potential Theory. Numerische Mathematik, 11 77, 1968.

6. Barnard, A.C.L., Duck, I. M., Lynn, M. S. and Timlake, W. P. The Application of Electromagnetic Theory to Electrocardiology. Biophys. J., 7 463, 1967.

7. The 3-D mesh generator is adapted from code written by W.C.T. Stoddart.

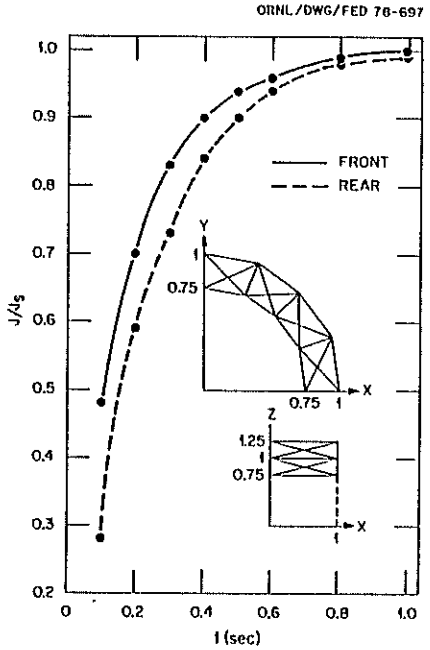

Fig. 1. Time history of eddy current in a circular ring.

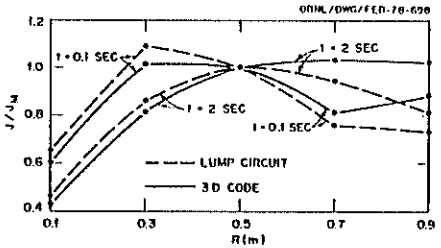

Fig. 2. Spatial profile of eddy current in a square plate.

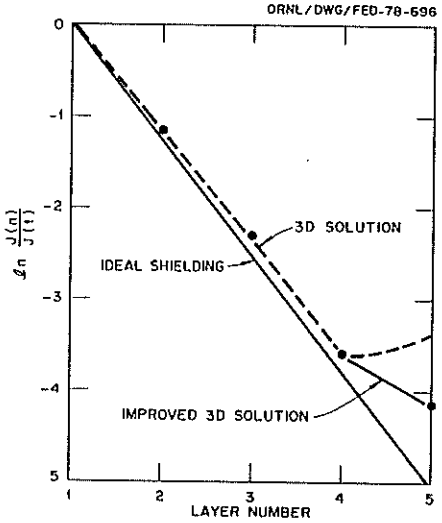

Fig. 3. Shielding of an oscillating dipole by a square plate.

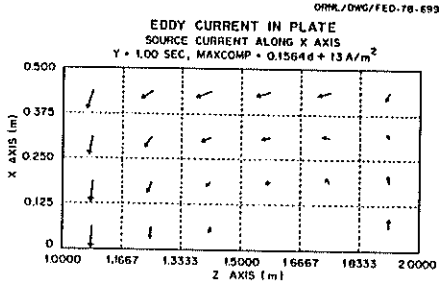

Fig. 4. Eddy pattern in a plate with Type 4 symmetry.

ETUDE EN 3D D'UN FOUR A INDUCTION DE RECHAUFFAGE DE PIECES DE SECTION RECTANGULAIRE

A. FOGGIA
Laboratoire d'Electrotechnique
ECOLE CENTRALE DE LYON
BP 163 - 69130-ECULLY (France)

RESUME

Dans cet article, l'auteur utilise une méthode d'éléments finis pour l'étude de la répartition tridimensionnelle des grandeurs électromagnétiques dans un four à induction employé en sidérurgie. Après la mise en équation, particulière à ce type de four, le domaine de résolution est découpé en éléments tétraédriques et la résolution des équations ainsi discrétisées conduit aux valeurs du potentiel vecteur.

1 - Introduction

Le chauffage à induction a été utilisé depuis fort longtemps pour effectuer notamment des traitements thermiques superficiels de certaines pièces en construction mécanique. Son utilisation était toutefois relativement limitée.

On assiste actuellement à un regain d'intérêt de ce type de chauffage grâce aux avantages que présente l'électricité comme source d'énergie par rapport aux autres sources d'énergie.

Le principe de fonctionnement de ces fours consiste à faire circuler dans la pièce à chauffer des courants électriques induits. Les pertes engendrées par ces courants de Foucault élèvent la température de la pièce jusqu'à la valeur désirée pour effectuer un laminage ou un formage -environ 1200°C-

Physiquement, un four à induction comprend des inducteurs à l'intérieur desquels se trouve la pièce à chauffer qui dans notre cas sera un parallélépipède. L'étude d'un tel dispositif est complexe car les phénomènes électromagnétiques, non linéaires dans le cas de l'acier, sont couplés aux phénomènes thermiques et au changement d'état qui intervient lors du franchissement du point de Curie.

Le but de cet article est de montrer les résultats de l'application d'une méthode d'éléments finis tridimensionnelle à l'étude d'un four à une température donnée. Le calcul présenté permet l'évaluation des puissances actives et réactives mises en jeu et constitue une étape préliminaire à la simulation du four en cours de fonctionnement.

2 - Mise en Equation

Le four qui fait l'objet de cette étude est schématisé à la Fig. 1. Il est constitué d'une bobine qui forme l'inducteur dont les spires sont de forme rectangulaire; la pièce à chauffer est un parallélépipède rectangle.

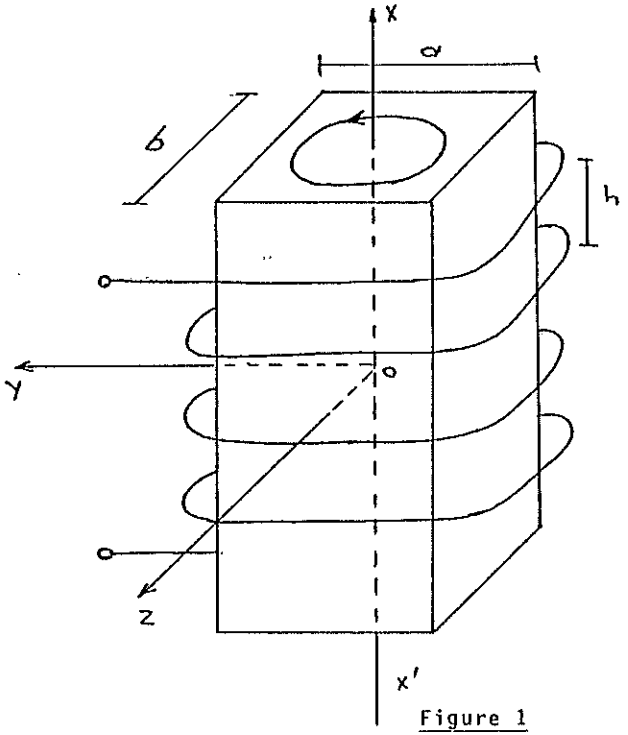

Figure 1

Dans le cas particulier de cette étude, nous supposerons que le pas h des inducteurs est petit par rapport aux dimensions a et b du noyau. Ainsi, on peut admettre que les courants de Foucault qui se développent dans le noyau sont situés dans des plans perpendiculaires à l'axe X'X

de la pièce, ainsi que le représente la figure 1.

Désignons par

$\vec{B}$: l'induction magnétique
$\vec{H}$: le champ magnétique
$\vec{A}$: le potentiel vecteur
$\vec{E}$: le champ électrique
$\vec{J}$: la densité des courants de Foucault
$\vec{J}_{ex}$: la densité des courants dans les inducteurs

σ la conductibilité électrique du noyau
μ la perméabilité magnétique du noyau
μ_o la perméabilité du vide

Toutes les grandeurs vectorielles sont fonction des variables d'espace (x, y, z), et du temps t.

Les équations de Maxwell s'écrivent :

$$\left.\begin{aligned} \operatorname{div} \vec{B} &= 0 \\ \operatorname{rot} \vec{H} &= \vec{J} + \vec{J}_{ex} \\ \operatorname{rot} \vec{E} &= -\frac{\partial \vec{B}}{\partial t} \\ \vec{J} &= \sigma \vec{E} \\ \operatorname{rot} \vec{A} &= \vec{B} \end{aligned}\right\} \qquad (1)$$

En combinant l'ensemble des équations (1), on aboutit à une équation unique dans laquelle seul intervient le potentiel vecteur $\vec{A}$:

$$\operatorname{rot}\left(\frac{1}{\mu} \operatorname{rot} \vec{A}\right) = -\sigma \frac{\partial \vec{A}}{\partial t} + \vec{J}_{ex} \qquad (2)$$

A cette équation, nous imposons la condition

$$\operatorname{div} \vec{A} = 0. \qquad (3)$$

Dans le problème qui nous concerne, le potentiel vecteur $\vec{A}$ ne possède que deux composantes dirigées suivant les axes Oy et Oz de la Fig.1 et que nous désignerons respectivement par $A_y(x,y,z,t)$ et $A_z(x,y,z,t)$.

Pour résoudre l'équation (2), nous avons utilisé une méthode que nous avons déjà employée pour des problèmes bidimensionnels [1], [2]. Il s'agit d'appliquer à l'équation (2) une projection de Ritz Galerkin associée à un découpage tétraédrique du domaine de résolution.

3 - Mise sous forme variationnelle et discrétisation

Le domaine de résolution est découpé en éléments tétraédriques à l'intérieur desquels nous pouvons écrire :

$$\vec{A}(x,y,z,t) = \sum_{j=1}^{N} \xi_j(x,y,z)\, \vec{A}_j(t) \qquad (4)$$

où les fonctions $\xi_j(x,y,z,t)$ constituent les fonctions de forme. Parmi les nombreuses fonctions ξ_j possibles, nous avons choisi des fonctions du 1° ordre définies par

$$\xi_j(x,y,z) = a_j + b_j x + c_j y + d_j z \qquad (5)$$

où les constantes a_j, b_j, c_j, d_j sont calculées à partir du système défini par

$$\begin{vmatrix} 1 & 1 & 1 & 1 \\ x_1 & x_2 & x_3 & x_4 \\ y_1 & y_2 & y_3 & y_4 \\ z_1 & z_2 & z_3 & z_4 \end{vmatrix} \begin{Vmatrix} \xi_1 \\ \xi_2 \\ \xi_3 \\ \xi_4 \end{Vmatrix} = \begin{vmatrix} 1 \\ x \\ y \\ z \end{vmatrix} \qquad (6)$$

Les éléments qui interviennent dans la matrice du système d'équations (6) sont les coordonnées des sommets de chaque tétraèdre élémentaire (Fig. 2)

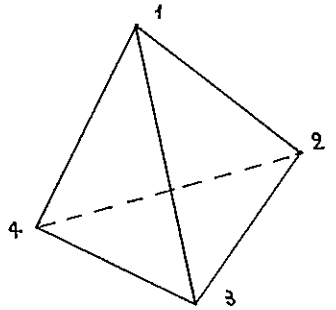

Figure 2

L'utilisation d'éléments du 1° ordre est intéressante car l'induction y est constante à l'intérieur et par conséquent la perméabilité magnétique l'est aussi.
Dans ces conditions, l'équation (2) appliquée à l'intérieur d'un tétraèdre élémentaire peut s'écrire

$$\frac{1}{\mu}\Delta\vec{A} = \sigma\frac{\partial\vec{A}}{\partial t} - \vec{J}_{ex} \qquad (7)$$

En effectuant une projection de Ritz-Galerkin au moyen des fonctions de forme [3]on obtient alors au noeud j :

$$\frac{1}{\mu}\int\left(\frac{\partial\vec{A}}{\partial x}\cdot\frac{\partial\zeta_j}{\partial x} + \frac{\partial\vec{A}}{\partial y}\cdot\frac{\partial\zeta_j}{\partial y} + \frac{\partial\vec{A}}{\partial z}\cdot\frac{\partial\zeta_j}{\partial z}\right)dV + \sigma\int\frac{\partial\vec{A}}{\partial t}\zeta_j dV = \int\vec{J}_{ex}\zeta_j dV \qquad (8)$$

L'ensemble des équations (8) conduit à un système différentiel qui est résolu par une méthode implicite.

4 - Conditions aux limites

Les équations (8) doivent être résolues dans le domaine représenté à la figure 3.

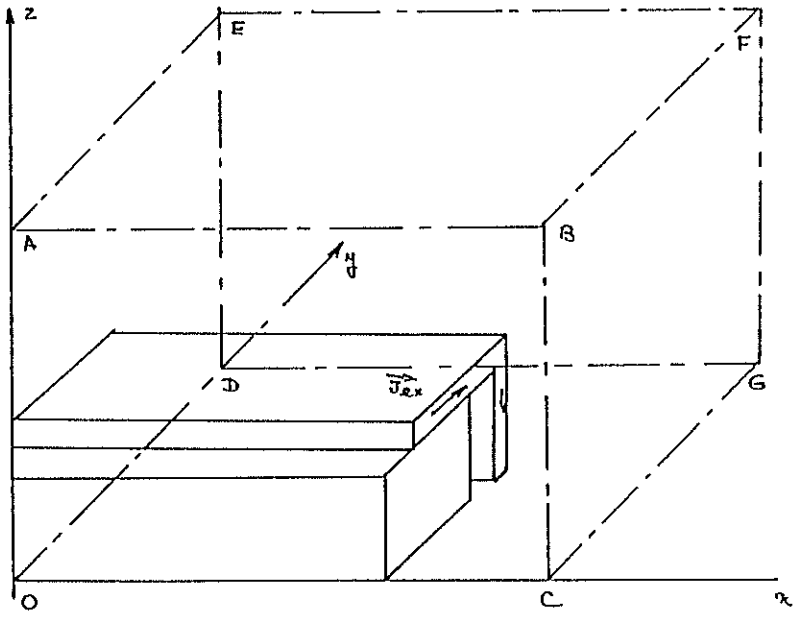

Figure 3

Il s'agit d'un parallélépipède à l'intérieur duquel se trouve le four. Les frontières ont été choisies de telle sorte que les plans OAED, OABC et OCDG constituent les trois plans de symétrie du four. En chaque point de ces trois plans, nous avons la condition

$$\frac{\partial\vec{A}}{\partial n} = 0 \qquad (9)$$

Ceci implique nécessairement sur l'axe Ox

$$\vec{A} = 0 \qquad (10)$$

Enfin, sur les autres surfaces : AEBF, DEFG, CBFG, nous avons imposé des conditions de Neumann exprimées par la relation (9).

L'équation vectorielle (8) se décompose en deux équations scalaires ; les conditions aux limites (9) et (10) se décomposent chacune en 2 conditions sur les composantes $A_y(x,y,z,t)$ et $A_z(x,y,z,t)$. Ainsi, nous avons donc à résoudre deux équations qui sont du type potentiel scalaire dont la solution est unique. Il en résulte donc que la solution de l'équation vectorielle (8) associée aux conditions aux limites (9), (10) est également unique.

5 - Résolution, Résultats

L'ensemble des équations (8) donne lieu à un système d'équations différentielles du type

$$M\frac{d\vec{A}}{dt} + N\vec{A} = \vec{S} \qquad (11)$$

En posant

$$\frac{d\vec{A}}{dt} = \frac{1}{\Delta t}\left(\vec{A}^{\,n+1} - \vec{A}^{\,n}\right) \qquad (12)$$

L'équation (11) exprimée à l'instant $(n+1)\Delta t$ s'écrit

$$\left(\frac{M}{\Delta t} + N\right)\vec{A}^{n+1} = \vec{S}^{n+1} + \frac{M}{\Delta t}\vec{A}^{n} \qquad (13)$$

dont la résolution à chaque instant a été effectuée au moyen d'une méthode de Gauss-Seidel par blocs.

Ce calcul a été utilisé pour l'étude de la répartition de l'induction dans un four de 1m de long qui chauffe des billettes carrées de 10 cm de côté. Le courant dans les inducteurs est à la fréquence de 50 Hz. La figure 3 montre l'intersection des surfaces d'induction par deux plans de symétrie.

11/77
320283

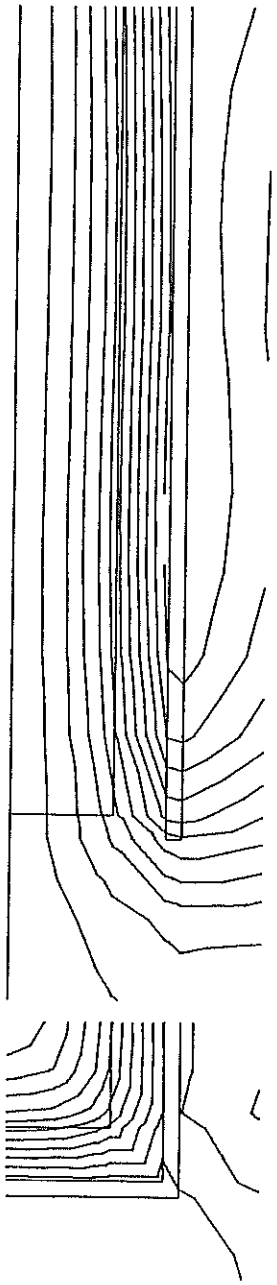

Figure 4

6 - Conclusion

Le calcul que nous venons de présenter permet l'étude détaillée d'un four à induction. L'utilisation d'une méthode d'éléments finis tridimensionnelle appliquée à ce type de problème présente l'avantage de conduire à une analyse fine des phénomènes et par conséquent à une bonne simulation du four.

Bien que le temps de calcul soit, d'une manière générale, relativement important, la forme simple du four ne nécessite qu'un nombre raisonnable d'éléments. Il en résulte alors que le temps de calcul demeure acceptable bien qu'assez long actuellement.

Les résultats présentés dans cet article constituent une première étape dans l'étude des fours ; en effet, à partir des grandeurs électromagnétiques ainsi calculées, il est possible de connaître la puissance dissipée en chaque point et par conséquent la température de la pièce chauffée.

7 - Références

(1) A. FOGGIA,J.C.SABONNADIERE,P.SILVESTER. Finite Element Analysis of travelling magnetic field problems. I.E.E.E. Trans. on Power App. and Systems May/June 1975 p.866-871

(2) A.FOGGIA. Finite Element analysis of a Single Sided Linear Induction motor. International Conference on Computer Aided design. S.Margherita Ligure (Italy) June 1976.

(3) O.C.ZIENKIEWICZ. La méthode des éléments finis. Ediscience 1973.